Binding of Organophosphorus Nerve Agents and

Their Simulants to Metal Salts

Jake Gold<sup>1</sup>, Tibor Szilvási<sup>1</sup>, Nicholas L. Abbott<sup>2</sup>, Manos Mavrikakis<sup>1,\*</sup>

<sup>1</sup>Department of Chemical and Biological Engineering, University of Wisconsin – Madison,

Madison, WI 53706

<sup>2</sup>Smith School of Chemical and Biomolecular Engineering, Cornell University, Ithaca, NY 14853

\*Corresponding author: Manos Mavrikakis (emavrikakis@wisc.edu)

**ABSTRACT:** Nerve agents (NAs) pose a great threat to society because they are easy to produce and are deadly in nature, which makes developing methods to detect, adsorb, and destroy them crucial. To enable development of these methods, we report the use of first principles electronic structure calculations to understand the binding properties of NAs and NA simulants on metal-salt surfaces. We report calculated Gibbs free binding energies ( $G_{BE}$ ) for four NAs (tabun ( $G_{A}$ ), sarin ( $G_{A}$ ), soman ( $G_{A}$ ), and venomous X ( $G_{A}$ ) and five NA simulants (dimethyl methylphosphonate ( $G_{A}$ ), dimethyl chlorophosphate ( $G_{A}$ ), trimethyl phosphate ( $G_{A}$ ), methyl dichlorophosphate ( $G_{A}$ ), and di-isopropyl methylphosphonate ( $G_{A}$ ) on metal-perchlorate and metal-nitrate salts using density functional theory. Our results indicate a general trend in the binding strength of NAs and NA simulants to metal-salt surfaces:  $G_{A}$ 0 on salt surfaces, we identify

the most effective simulant for each of the studied NAs as follows: DMCP for GA, TMP for GB and GD, and DMMP for VX. To illustrate the utility of the binding energies calculated in our study, we address the design of NA sensors based on competitive binding of NAs and liquid-crystalline compounds on metal salts. We compare our results with previous experimental findings and provide a list of promising combinations of liquid-crystal and metal-salt systems to selectively and sensitively detect NAs. Our study highlights the great value of computational chemistry for designing selective and sensitive NAs sensors while minimizing the number of very dangerous experiments involving NAs.

**KEYWORDS:** liquid crystals, nerve agents, coordination interactions, optical materials, gas sensor, density functional theory

#### 1. INTRODUCTION

Chemical warfare agents (CWAs), especially nerve agents (NAs), are some of the most lethal compounds ever synthesized. The synthesis and storage of CWAs are strictly prohibited worldwide by the Chemical Weapons Convention (CWC) arms-control treaty to which 193 states are party. Nevertheless, there are still well-documented examples of CWA usage (e.g., recent events in Syria and Iraq) and a few nations have yet to sign and/or ratify the CWC. Therefore, the detection, adsorption, and destruction of CWAs remains a relevant and unresolved problem. Advancements in the development of portable solutions and their implementation in, for example, unmanned vehicles may enable the detection of trace concentrations of CWAs and reveal their usage to deter future incidents involving CWAs.

Because of the great danger posed by NAs, there are many prospective or developed technologies to monitor and neutralize NAs. Successful examples for monitoring NAs using optical methods, <sup>3,4</sup> gas chromatography, <sup>4,5</sup> ion mobility or mass spectrometry, <sup>4,5</sup> and molecularlevel chemical sensing<sup>6-8</sup> have been demonstrated. While technologies based on gas chromatography can be highly sensitive and selective to NAs, they are also often slow, require power supplies and involve heavy instrumentation (preventing, for example, monitoring of personal exposure). One type of sensing innovation to overcome these limitations is molecular level sensing, which utilizes relevant chemistry to integrate sampling, pretreatment and measurement. These chemical sensing approaches often require novel materials that can bind or react with NAs. 9,10 Strong binding of NAs is also relevant to NA capturing applications, which is important because, particularly at low temperatures, persistence of certain NAs in the environment can last up to 2-4 weeks. 11 Destruction of NAs generally builds on chemical reactivity such as the hydrolysis of NAs and NA simulants. For example, metal-organic frameworks<sup>12,13</sup> or metal oxides<sup>14,15</sup> have been used as catalysts for hydrolysis of NAs and NA simulants. The first step in the destruction of NAs using these materials is adsorption. However, NA destruction also involves other elementary processes, including bond-breaking events within the analyte, leading to the analyte's decomposition. Such processes may limit the entire NA destruction process. As a result, studying the thermochemistry and kinetics of these bond-breaking events would be essential for designing improved materials for the destruction of NA's. The first step in the destruction of NAs using these materials is adsorption, and often steps involving bond breaking can scale with the adsorption energy in heterogeneous catalysis.

Importantly, many of these NA sensing, capture, and destruction technologies build on the binding of organophosphates via the phosphoryl group to metal cations. <sup>16,17</sup> Therefore,

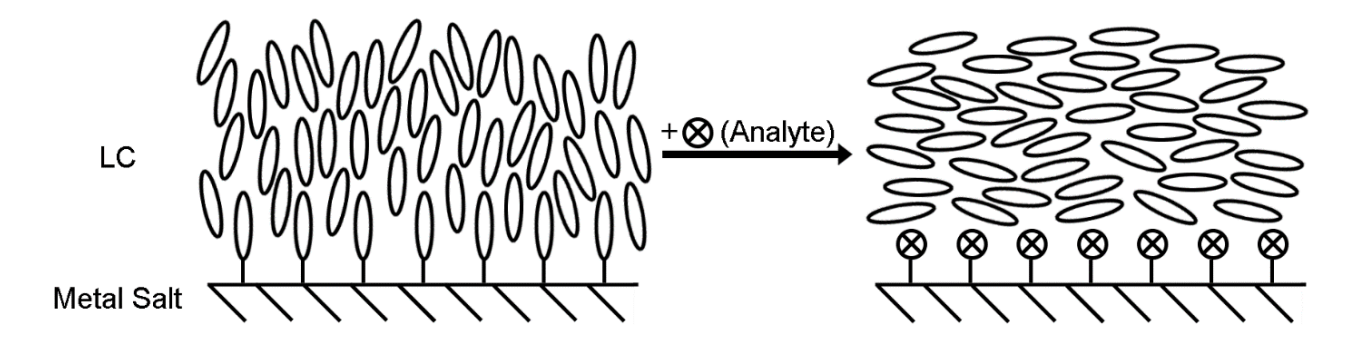
understanding the interaction of NAs and NA simulants on various solid ionic surfaces is of fundamental importance. Here, we propose to use computational chemistry methods to gain insights into this interaction for several reasons: NA molecules are dangerous to handle, highly restricted in their availability and thus challenging compounds for experimentation. These limitations have generally resulted in experiments being performed with simulants that typically represent well only a subset of NA properties. Accordingly, through the implementation of thoroughly evaluated computational models for NA adsorption on solid surfaces, computations can offer access to insights into the interactions of NA themselves as opposed to NA-simulant molecules on the same surfaces. In addition, the efficiency of a computational model also makes possible exploration of a range of molecules and surfaces that is much greater than what is practical to examine with experiments. To demonstate how electronic structure computational methods can reveal fundamental insights into the interaction of NAs with solid surfaces, we choose to study metal-salt surfaces here, which have been used in chemoresponsive liquid crystalline materials. which have been used in chemoresponsive liquid crystalline materials. In previous work, we have shown that metal salts can be utilized for the adsorption of NAs, 18,19 via strong binding to metal cations. 16,17 Further, the choice of anion in the salt surfaces has been shown to influence the strength of this interaction. <sup>20,21</sup> As a result, there is a large combination of cations and anions that could be used with salt surfaces for the adsorption, detection, capture and potential destruction of NAs.

As an illustration on how computational chemistry can guide and accelerate the development of novel technologies for the detection, capture, and destruction of NAs, we analyze the potential detection of NAs using chemoresponsive liquid crystalline based sensors.<sup>22,23</sup> Liquid crystals (LCs) are phases of matter within which molecules exhibit preferred orientations (director) that

can be selected by interactions with interfaces <sup>16,17,30,31,19,22,24–29</sup> or external fields. <sup>32–34</sup> For example, Shah and coworkers revealed that the alignment of LCs on metal-salt substrates is strongly dependent on the coordination of specific functional groups of the LC molecules (mesogens) to the metal-salt surface. 23 Specifically, the nematic LC phase of 4'-n-pentyl-4-biphenylcarbonitrile (5CB; Scheme 1) supported on certain metal-perchlorate-decorated surfaces, such as Al(ClO<sub>4</sub>)<sub>3</sub> or Ni(ClO<sub>4</sub>)<sub>2</sub>, shows a homeotropic orientation (molecules oriented perpendicular to the surface normal; Scheme 2, left), a consequence of the coordination of the nitrile functional group of 5CB to the metal cations on the surface.<sup>31</sup> In the presence of a target analyte that binds more strongly to the metal cation than the mesogen, the interaction between the mesogens and the surface is disrupted and changes the director to an orientation parallel to the surface (Scheme 2, right). This shift in the LC orientation can then be detected by optical methods. This general principle is only valid if displacement of the mesogen at the surface is favored, which can be calculated from DFT based on the competitive binding of the mesogen and the analyte. Therefore, binding free energy calculations can be particularly insightful for this type of chemoresponsive materials. Using this general principle, several different analytes (e.g., H<sub>2</sub>S, <sup>35</sup> NO<sub>2</sub>, <sup>36</sup> trimethylamine, <sup>37</sup> CO<sub>2</sub>, <sup>38</sup> Cl<sub>2</sub>, <sup>24,39</sup> and organophosphates<sup>9,10,11–18,19,20,28,29</sup>) have been shown to induce a chemoresponse in tailored LC-based materials supported on metal salts or other surfaces.

**Scheme 1.** Molecular structure of mesogens studied: "5CB" – 4'-n-pentyl-4-biphenylcarbonitrile, "PM" – 5-(4-pentylphenyl)-pyrimidine, and "PD" – 4-(4-pentylphenyl)-pyridine. The corresponding surrogate

molecule for each of these mesogens used in the computations are shown directly to the right of the vertical line: benzonitrile (for 5CB), pyridine (for PM), and pyrimidine (for PD).

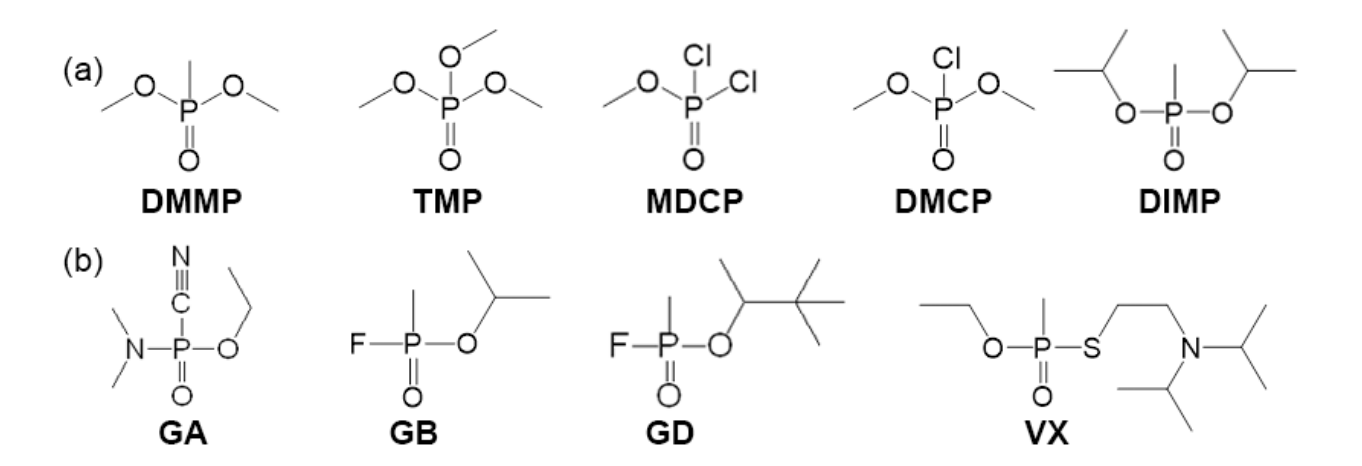


**Scheme 2.** A schematic illustration demonstrating the principle of analyte detection based on competitive binding between an analyte and a mesogen for a metal cation binding site on a surface. The mesogens can form strong bonds with the metal cations, inducing a homeotropic orientation in the bulk of the nematic LC (left). When the LC is exposed to a stronger-binding analyte, the analytes displace the mesogens at the surface and a homeotropic-to-planar transition of the LC is triggered (right).

Recently, we developed computational models to understand and predict the interaction of different mesogens and analytes with metal-salt surfaces. <sup>16,17,21,25</sup> Despite the relative simplicity of our atomistic models, we found excellent agreement with experimental chemoresponse measurements, which led to the first-ever computational design of a chemoresponsive LC-based system. <sup>17</sup> Furthermore, we have shown how electronic-structure calculations can guide the design of increased water-tolerant LC-based sensors <sup>16</sup> and have expanded the list of relevant metal-salt substrates by showing that nitrates can also be useful in chemoresponsive applications. <sup>21</sup> Guided by computational chemistry, we also elucidated a new detection principle capitalizing on the redox properties of metal salts. <sup>24</sup> Most recently, we have shown that similar computational methods can guide detection on metal films using a competitive binding interaction. <sup>39</sup>

Building on our previous successful application of computational chemistry methods, and motivated by the observation that the value of efficient and accurate computational-chemistry methods becomes particularly high when dealing with detection of toxic compounds, here we focus on the adsorption behavior of NAs to metal salts and the design of chemoresponsive LC systems for detection of NAs. We note that only one experimental study has reported on the

responses of LCs to real NAs and, in that study, only a limited number of metal salts and mesogens were investigated. <sup>19</sup> In contrast, to mitigate safety concerns, other studies have used less toxic NA simulants that share select similarities (in terms of physico-chemical properties) to real NAs. <sup>42,43</sup> A number of NA simulants have been reported in the literature (Scheme 3a), <sup>44</sup> but dimethyl methylphosphonate (DMMP) is the most commonly used NA simulant. <sup>42,43</sup> Our approach to making predictions for chemoresponsive LCs of the NAs in Scheme 3 is to focus on the binding free energy calculations because the mechanism in Scheme 2 is based on a displacement event. However, transport of the analyte from air to the surface through the LC is another important process which could affect the response time of the chemoresponsive system. The transport process is influenced by diffusion and partition coefficients. <sup>27,45</sup> For the case of the NA simulant DMMP, we have found many examples where increasing the magnitude of the displacement energy typically decreases the response time. <sup>21</sup> Our approach is to assume a similar case for all the analytes in Scheme 3, specifically that a larger displacement energy allows for the design of faster and more sensitive chemical sensors.



**Scheme 3.** Chemical structures of (a) NA simulants and (b) NAs. The NA simulants are described by their acronym: dimethyl methylphosphonate (DMMP), trimethyl phosphate (TMP), methyl dichlorophosphate (MDCP), dimethyl chlorophosphate (DMCP), and di-isopropyl\_methylphosphonate (DIMP). The NAs are

described by their two letter North-Atlantic Treaty Organization (NATO) identifier: tabun (GA), sarin (GB), soman (GD), and venomous X (VX).

This work seeks to develop a database for the binding properties of NAs and NA simulants to commonly available metal salts. Our goal is threefold: (i) determine important trends in how NAs and NA simulants bind to metal-salt substrates, (ii) identify the best NA simulant for each NA based on binding properties, and (iii) guide the development of LC-based sensitive and selective chemoresponsive systems for the detection of real NAs with metal-salt surfaces. The database reported herein has the potential to help researchers reduce the time needed to develop LC-based NA sensors.

To understand the interaction of NAs and NA simulants with metal-salt surfaces in general, we study the binding properties of four common NAs (sarin (GB), soman (GD), tabun (GA), and venomous X (VX); Scheme 3b) and five established NA simulants (DMMP, dimethyl chlorophosphite (DMCP), trimethyl phosphate (TMP), methyl dichlorophosphate (MDCP), and di-isopropyl methylphosphonate (DIMP); Scheme 3a). We calculate the binding free energies of these molecules to commonly available metal salts composed of 12 metal cations (AI<sup>3+</sup>, Cd<sup>2+</sup>, Co<sup>2+</sup>, Cr<sup>3+</sup>, Cu<sup>2+</sup>, Fe<sup>3+</sup>, Ga<sup>3+</sup>, La<sup>3+</sup>, Mn<sup>2+</sup>, Ni<sup>2+</sup>, Sc<sup>3+</sup>, and Zn<sup>2+</sup>) and two anions (ClO<sub>4</sub><sup>-</sup> and NO<sub>3</sub><sup>-</sup>), thereby providing a comprehensive picture on the binding of NAs and NA simulants to various metal salts. We also compare the calculated binding strengths of the NAs and NA simulants with three mesogens previously studied for DMMP detection with metal-salt systems <sup>16</sup> ("5CB" – 4'-n-pentyl-4-biphenylcarbonitrile, "PD" – 4-(4-pentylphenyl)-pyridine, and "PM" – 5-(4-pentylphenyl)-pyrimidine; Scheme 1) to identify the most responsive LC-based system for detection of real NAs.

In this work, we show that the binding strengths of NAs and NA simulants depend on the specific molecule involved (up to 0.88 eV on Sc(ClO<sub>4</sub>)<sub>3</sub>) as well as the identity of the metal cation, providing opportunities to develop selective sensors to distinguish individual NAs and NA

simulants. However, the large differences in binding strengths also suggest that DMMP, used almost exclusively in experiments as a NA simulant, does not provide an accurate picture of the binding properties of all the NAs considered here. We elucidate a trend in the binding free energy (G<sub>BE</sub>) of NAs and their simulants nearly independent from the metal salt with binding strengths increasing in the following order: MDCP < DMCP < GA < GD ~ GB < TMP < VX ~ DMMP < DIMP. According to this analysis, which clearly does not address all important factors needed for a complete design (e.g.: partition function and transport of analytes in LC phases), we find that the relative ordering of G<sub>BE</sub> values indicates that DMMP is a good simulant for binding of VX to metal salts. However, chemoresponsive systems designed based on experiments with the simulant DMMP may not respond to GA, GD, or GB because of their weaker than DMMP binding to metal salts. Based on similar binding energies, we show that the following represent more accurate pairs of (NA-simulant, NA): (DMCP, GA), (TMP, GD or GB), and (DMMP, VX). In addition, we predict that sensors designed using MDCP or DMCP as test compounds can respond to all NAs. Overall, the database of binding strengths derived here can serve as a starting point for designing sensitive and selective LC-based devices chemoresponsive to real NAs.

#### 2. COMPUTATIONAL METHODS

Density functional theory (DFT) calculations were carried out using the *Gaussian 09 D.01* code. Geometry optimizations were performed with the PBE exchange-correlation functional together with Grimme's D3 empirical dispersion correction without damping function (D3) and a def2-SVP basis set. Thermodynamic correction terms were calculated at 298.15 K, using the same level of theory. To obtain more accurate energetics, starting from the optimized geometries, single-point calculations were performed with the M06-2X-D3 hybrid functional and a larger def2-TZVP basis set. Thermodynamic correction terms calculated at the PBE/def2-SVP level of

theory were added to these more accurate energies to obtain Gibbs free energies at room temperature and 1 atm pressure.

For metal-perchlorate and metal-nitrate salts, calculations were performed using the Neutral Anion Model (NAM) described in detail elsewhere. 16,17,21 We briefly discuss the main features of the NAM model here. The NAM is a cluster model reflecting the stoichiometry of the metal salts used in experiments. Figure 1 shows representative examples of the NAM for three metal salts: Al(ClO<sub>4</sub>)<sub>3</sub>, La(ClO<sub>4</sub>)<sub>3</sub>, and Cu(NO<sub>3</sub>)<sub>2</sub>. To model the Al(ClO<sub>4</sub>)<sub>3</sub> metal salt, we use one Al<sup>3+</sup> cation and add three ClO<sub>4</sub> anions to neutralize the Al<sup>3+</sup> center (Figure 1a, left). In the energetically most favorable structure, each perchlorate anion forms two bonds with two of the available six coordination sites of Al<sup>3+</sup>. To simulate the binding interactions of the mesogen or targeted analyte, the relevant functional group of either the mesogen or the analyte has to bind to the metal center. For the case of Al3+, which has only six available coordination sites, one aluminum-perchlorate bond has to break to accommodate a new metal-center mesogen/analyte bond (Figure 1a, middle and right). A similar model is used for the other tertiary charged metal cations with six available coordination sites: Cr<sup>3+</sup> and Ga<sup>3+</sup>. Although La<sup>3+</sup>, Fe<sup>3+</sup>, and Sc<sup>3+</sup> have a structurally similar model to Al<sup>3+</sup> (Figure 1b, left), these metal cations can form more than six coordinations owing to their empty d- and f-shells. Therefore, mesogens or analytes can coordinate to the metal cation without breaking a cation-anion bond (Figure 1b, middle and right) in those cases. Metals with a 2+ charge state (Cd<sup>2+</sup>, Co<sup>2+</sup>, Cu<sup>2+</sup>, Mn<sup>2+</sup> Ni<sup>2+</sup>, and Zn<sup>2+</sup>) are neutralized with two anions, where each anion forms two bonds with the metal cation (Figure 1c, left). Metal cations with a 2+ charge can also form a coordinative interaction with mesogens or analytes without breaking a metal-perchlorate bond (Figure 1c, middle and right).

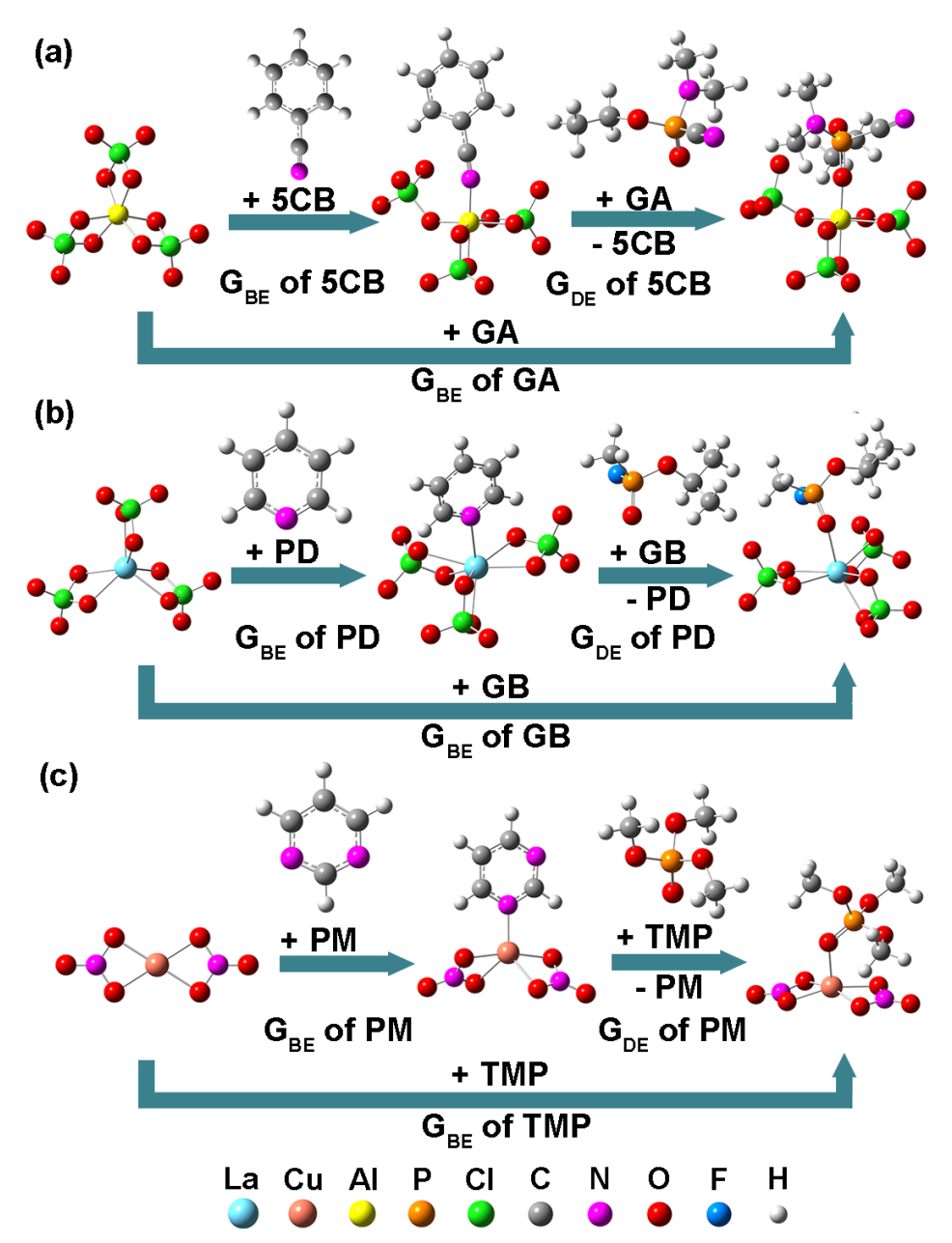


**Figure 1.** Representative optimized structures for the binding free energy  $(G_{BE})$  and displacement free energies  $(G_{DE})$  calculations. (a) Cluster model for  $Al(ClO_4)_3$  (left) and its binding with benzonitrile (middle) and GA (right). (b) Cluster model for  $La(ClO_4)_3$  (left) and its binding with pyridine (middle) and GB (right). (c) Cluster model for  $Cu(NO_3)_2$  (left) and its binding with pyrimidine (middle) and TMP (right). Color code used for atoms: green -Cl; red -O; pink -N; dark grey -C; light silver -H; yellow -Al; light blue -La; salmon -Cu; dark blue -F; and orange -P.

We emphasize that the NAM model is defined for each metal salt by stoichiometry described above rather than calculating the most stable configuration under specific conditions such as at a

given relative humidity (RH). We address the stability of the metal perchlorate salts in the Supporting Information (SI) including the dissociation of the metal perchlorate salt cluster (Table S1), the displacement of the perchlorate ion by water (Table S2), and the displacement of the perchlorate ion by deprotonated water (Table S3). In general, the NAM was found to be more stable than structures where water or solvent displaces a perchlorate ion which could reflect experimental conditions (detailed description in the SI). However, at high RH, it could be possible to have water as an additional ligand in the coordination environment. We have studied this aspect of the influence of water in a previous publication<sup>21</sup> and found that inclusion of water in the ligand environment tends to change the absolute G<sub>BE</sub> while the relative G<sub>BE</sub> order for various adsorbates (e.g.: liquid crystals, analytes) was not influenced. This is likely why the NAM captures very well the experimental response in chemoresponsive liquid crystal experiments.

To maximize the computational efficiency when calculating Gibbs free binding energies (G<sub>BE</sub>) of the mesogen to the metal-salt clusters, we represent mesogens with a truncated surrogate molecule that has a similar binding energy. We have previously verified that benzonitrile, pyridine, and pyrimidine are good surrogate molecules for the following LCs: 5CB, PD, and PM (Scheme 1), respectively. The Gibbs free binding energy (G<sub>BE</sub>) of a mesogen or analyte adsorbate is calculated as

$$G_{BE} = G_{sub+ads} - G_{sub} - G_{ads}$$
 (1)

where  $G_{\text{sub+ads}}$  is the total Gibbs free energy of the adsorbate bound to the metal-salt-cluster substrate,  $G_{\text{sub}}$  is the Gibbs free energy of the metal-salt-cluster substrate, and  $G_{\text{ads}}$  is the Gibbs free energy of the adsorbate in the gas phase (e.g., surrogate LC molecule or analyte). We have shown in previous studies that large negative  $G_{\text{BE}}$  values for mesogen surrogates suggest that a homeotropic orientation is preferred, whereas positive values point to a planar orientation.  $^{16,21}$ 

While it may be possible to bind multiple mesogens or analytes to one metal salt cluster, we only report the G<sub>BE</sub> of binding one mesogen or analyte to each cluster. We emphasize that our model was developed to compare results with experimentally synthesized metal salt surfaces, which would likely have additional steric constraints (compared to the NAM cluster model) that may limit the number of mesogens or analytes that could bind to one cation to one. We Next, we define the displacement free energy (G<sub>DE</sub>) as:

$$G_{DE} = G_{BE-analyte} - G_{BE-LC}$$
 (2)

where G<sub>BE-analyte</sub> and G<sub>BE-LC</sub> are the Gibbs free binding energy of the targeted analyte and of the mesogen, respectively. In general, more negative G<sub>DE</sub> values indicate a larger thermodynamic driving force for displacement of the mesogen by the analyte. We have shown previously that good agreement with experiments is found if G<sub>DE</sub> is more negative than a threshold value (i.e.: just negative sign of G<sub>DE</sub> is not enough),<sup>16,21</sup> and that the magnitude of G<sub>DE</sub> correlates well with the response time of LC-based chemoresponsive systems. In addition, we have found a universal exponential relationship between calculated G<sub>DE</sub> values and the experimental response time to DMMP, which is agnostic of anion and cation identity.<sup>21</sup>

#### 3. RESULTS AND DISCUSSION

We present the adsorption behavior of a total of nine analytes, four NAs (GA, GD, GB, and VX) and five NA simulants (MDCP, DMCP, TMP, DMMP, and DIMP), on metal salt surfaces composed of combinations of 12 metal cations (Al<sup>3+</sup>, Cd<sup>2+</sup>, Co<sup>2+</sup>, Cr<sup>3+</sup>, Cu<sup>2+</sup>, Fe<sup>3+</sup>, Ga<sup>3+</sup>, La<sup>3+</sup>, Mn<sup>2+</sup>, Ni<sup>2+</sup>, Sc<sup>3+</sup>, and Zn<sup>2+</sup>) and two anions (ClO<sub>4</sub><sup>-</sup> and NO<sub>3</sub><sup>-</sup>). This section is organized into four subsections: (1) binding properties of analytes to perchlorate salts, (2) binding properties of analytes to nitrate salts and comparison of the binding properties between perchlorate and nitrate

salts, (3) comparison to previously published experimental results, and (4) predictions for future experiments.

We report several calculated average quantities to characterize analyte binding. The following notation is used consistently for these quantities:  $\langle G_{BE} \rangle_{X,Y}$  refers to the Gibbs binding free energy averaged over set X (either A for analyte or C for cation), whereas Y indicates the relevant anion (P or N for perchlorates or nitrates, respectively). For example,  $\langle G_{BE} \rangle_{C,P}$  indicates the average Gibbs free binding energy of a specific analyte averaged over all metal cations for perchlorate salts, which can be used to understand general trends in the binding strength of the various analytes. Similarly,  $\langle G_{BE} \rangle_{A,N}$  refers to the Gibbs free binding energy for a particular metal cation averaged over all analytes (NAs and NA simulants) for nitrate salts, which is useful to quantify how strong a particular metal cation binds to these organophosphorus compounds. We use the same notation to define the average displacement Gibbs free energy (i.e.,  $\langle G_{DE} \rangle_{X,Y}$ ) (see Equation 2 for the definition of a displacement free energy).

#### 3.1. Binding properties of analytes to perchlorate salts

Figure 2 provides the  $G_{BE}$  for nine analytes with twelve metal-perchlorate salts. We order the analytes by increasing  $|\langle G_{BE}\rangle_{C, P}|$  from left to right (see bottom line entries in Fig. 2). Based on  $|\langle G_{BE}\rangle_{C, P}|$ , the general trend in binding strength for the studied NAs and NA simulants is:  $MDCP < DMCP \sim GA < GD \sim GB < TMP < VX \sim DMMP < DIMP$ . We define analytes as having similar binding strengths if their  $\langle G_{BE}\rangle_{C, P}$  is within 0.06 eV of each other, which reflects a difference of one order of magnitude in surface coverages at room temperature. For each case, we found that the most favorable binding occurred via the phosphoryl oxygen to the metal cation (Figure 1). Additionally, the overall trend in binding strength was found to be very similar to the

trend reported on silica determined by temperature programmed desorption: MDCP < DMCP < GB < GD < TMP < DMMP < DIMP. 44,51 We suggest that this similarity reflects the similar binding structures of NAs and NA simulants on different surfaces and the similar electron withdrawing properties of the ligands that influence the binding strength (see details further below).

The calculated  $\langle G_{BE} \rangle_{C, P}$  values show a large difference in binding properties among the different NAs and NA simulants. For example, the weakest- and strongest-binding analytes on the metal-perchlorate salts studied (MDCP and DIMP, respectively) have  $\langle G_{BE} \rangle_{C, P}$  values of -0.80 eV and -1.43 eV, respectively. This large difference in  $\langle G_{BE} \rangle_{C, P}$  between these two analytes (0.63 eV) demonstrates that the binding properties of each analyte can be vastly different. This conclusion is further supported by focusing on specific metal salts. For example, the difference in  $G_{BE}$  values between the weakest- and strongest-binding analyte to  $Sc(CIO_4)_3$  is 0.88 eV (see Figure 2, line of entries for  $Sc^{+3}$ ). Interestingly, the smallest difference in  $G_{BE}$  between the weakest- and strongest-binding analyte occurs for MDCP and DIMP on  $Cu(CIO_4)_2$ , but this difference in  $G_{BE}$  is still large: 0.48 eV (see Figure 2).

	MDCP	DMCP	GA	GD	GB	TMP	VX	DMMP	DIMP	<g<sub>BE&gt;<sub>A,P</sub></g<sub>	-0.20
Cu <sup>2+</sup>	-0.58	-0.68	-0.62	-0.74	-0.89	-0.85	-1.01	-1.08	-1.06	-0.83	-0.40
Cr <sup>3+</sup>	-0.53	-0.66	-0.72	-0.80	-0.76	-0.97	-1.01	-1.01	-1.14	-0.85	
Ga <sup>3+</sup>	-0.55	-0.88	-0.85	-1.05	-0.95	-1.07	-1.28	-1.30	-1.35	-1.03	-0.60
Al <sup>3+</sup>	-0.69	-0.80	-0.90	-0.99	-1.08	-1.15	-1.28	-1.34	-1.40	-1.07	-0.80 (0)
Fe <sup>3+</sup>	-0.69	-0.92	-1.00	-0.94	-1.02	-1.25	-1.16	-1.37	-1.33	-1.07	
Cd <sup>2+</sup>	-0.81	-0.97	-1.00	-1.03	-1.05	-1.19	-1.31	-1.28	-1.35	-1.11	-1.00
Ni <sup>2+</sup>	-0.89	-1.01	-1.12	-1.19	-1.18	-1.21	-1.20	-1.32	-1.43	-1.17	-1.00 land
Co <sup>2+</sup>	-0.88	-1.01	-1.11	-1.25	-1.25	-1.31	-1.33	-1.37	-1.46	-1.22	<b>J</b> C
Zn <sup>2+</sup>	-0.93	-1.10	-1.10	-1.23	-1.27	-1.29	-1.46	-1.37	-1.52	-1.25	-1.40 B
Mn <sup>2+</sup>	-0.99	-1.11	-1.12	-1.21	-1.28	-1.31	-1.45	-1.41	-1.49	-1.26	-1.60
Sc <sup>3+</sup>	-0.94	-1.00	-1.24	-1.30	-1.31	-1.53	-1.58	-1.62	-1.82	-1.37	-1.80
La <sup>3+</sup>	-1.08	-1.30	-1.24	-1.36	-1.32	-1.57	-1.56	-1.71	-1.80	-1.44	-1.00
<g<sub>BE&gt;<sub>C,P</sub></g<sub>	-0.80	-0.95	-1.00	-1.09	-1.11	-1.23	-1.30	-1.35	-1.43	-1.14	-2.00

**Figure 2.** Calculated binding free energy ( $G_{BE}$ ; in eV) for a total of nine analytes (NAs and NA simulants) on metal-perchlorate salts. The color scale demonstrates the relative strength of adsorption and ranges from red (weak binding) to green (strong binding), with yellow in between. NAs and NA simulants are arranged from left to right according to increasing  $G_{BE}$  averaged over all metal cations (bottommost row,  $G_{BE}$ ).

The cations are arranged from top to bottom by increasing  $G_{BE}$  averaged over all analytes (rightmost column,  $\{G_{BE}\}_{A,P}$ ).

Similar to NA simulants, NAs also show considerable differences in  $\langle G_{BE} \rangle_{C, P}$ . The NA with the largest  $\langle G_{BE} \rangle_{C, P}$  is VX (-1.30 eV) and the NA with the smallest  $\langle G_{BE} \rangle_{C, P}$  is GA (-1.00 eV). However, the magnitude of this difference can either decrease or increase depending on the particular metal salt to which the analyte is bound. For instance, the difference in  $G_{BE}$  between VX and GA on  $G_{AE}$  on  $G_{AE}$  is 0.43 eV, while the difference in  $G_{AE}$  between VX and GA on  $G_{AE}$  is 0.08 eV. However, we have previously shown that a difference of 0.05 eV in  $G_{AE}$  can lead to a chemoresponse or not, depending on the mesogen. Therefore, differences as small as 0.08 eV in  $G_{AE}$  can lead to significant differences in measurable quantities extracted from well-designed experiments. Further below, we discuss how the molecular and electronic structure of the analytes lead to these differences in binding energy.

The identity of the metal cation in the salt plays an important role in determining strength of binding for the analytes studied. In particular, the average Gibbs free binding energy over all analytes,  $\langle G_{BE} \rangle_{A, P}$  (see Figure 2), increases as follows:  $Cu^{2+} \langle Cr^{3+} \langle Ga^{3+} \langle Fe^{3+} \langle AI^{3+} \langle Cd^{2+} \langle Ni^{2+} \langle Co^{2+} \langle Zn^{2+} \langle Mn^{2+} \langle Sc^{3+} \langle La^{3+} \rangle$ . Importantly, our calculated  $\langle G_{BE} \rangle_{A, P}$  values show large differences in the binding properties between cations.- While the  $\langle G_{BE} \rangle_{A, P}$  for the strongest-binding cation  $La^{3+}$  is -1.44 eV, the  $\langle G_{BE} \rangle_{A, P}$  of the weakest-binding cation  $Cu^{2+}$  is only -0.83 eV. This difference is larger for some analytes; for example, the difference for DIMP between the weakest- ( $Cu^{2+}$ ) and strongest-binding ( $La^{3+}$ ) cation is 0.74 eV (see Figure 2). The choice of metal cation can therefore significantly impact the binding strength of analytes, which is in line with previous experimental studies with DMMP showing that the specific choice clearly influences the chemoresponsiveness of the LC system. <sup>52</sup> Depending on the nature of the selected metal cation,

the response time can change by two orders of magnitude for a given analyte on either perchlorate or nitrate salts. 16,21,25

The NA and NA simulants studied here have similar molecular structures (Scheme 3) which allows the quantification of the influence of different functional groups on the calculated  $\langle G_{BE} \rangle_{C}$ . P. For example, we quantify the effect of Cl and OCH<sub>3</sub> ligands on the binding properties of analytes by comparing the  $\langle G_{BE} \rangle_{C, P}$  of TMP (zero Cl and three OCH<sub>3</sub> ligands), DMCP (one Cl and two OCH<sub>3</sub> ligands), and MDCP (two Cl and one OCH<sub>3</sub> ligands). The |<G<sub>BE</sub>><sub>C,P</sub>| of TMP is 0.28 eV larger than that of DMCP, while the  $|\langle G_{BE} \rangle_{C,P}|$  of DMCP is 0.15 eV larger than that of MDCP (see Figure 2), suggesting that Cl substitution lowers the |G<sub>BE</sub>| of an analyte. The binding of MDCP, DMCP, and TMP to the metal cation of the salt surfaces occurs through the phosphoryl group. The electronegative Cl ligands can significantly influence the G<sub>BE</sub> by withdrawing the electron density from the phosphoryl group, thereby weakening the bond between the phosphoryl group and the metal salt. The effect of Cl groups can be visualized through electron-density-difference plots that show the change in electron density due to bond formation between the analyte and metal salt. Previous studies have indicated that a larger change in electron density (i.e., larger charge transfer) suggests stronger binding. <sup>21,16,17,25</sup> Figures 3a and 3b show the electron-density-difference plot for MDCP and TMP bound to Sc(ClO<sub>4</sub>)<sub>3</sub>, respectively. The cyan and purple regions in these plots, which indicate electron-density depletion and accumulation, respectively, are smaller for MDCP than for TMP. This result is consistent with the electron-withdrawing property of Cl that withdraws electron density from the P=O group. Thus, charge transfer from the P=O group to the metal cation is smaller in the case of MDCP as opposed to TMP, which explains the stronger binding of TMP compared to MDCP on the metal salts studied here.

We then study the adsorption of NA simulants MDCP and TMP on salt surfaces by using the charge difference plots in Figure 3a-b. The analysis described here for MDCP and TMP can be used to help understand the  $G_{BE}$  trends of NAs as well. For example, NAs also contain electronegative functional groups such as F, CN, ether, sulfide, or amino groups, which can explain the  $G_{BE}$  trend of NAs. Based on the arguments developed above we can rationalize why GA, which has three electronegative groups (CN, ether, and amino groups), binds the weakest of the NAs. In addition, GB and GD both have one highly electronegative F ligand and one ether group; thus they bind very similarly to each other but still stronger than GA to the metal salts. Lastly, VX has only two weakly electronegative groups, an ether and sulfide group, and thus binds the strongest among the NAs. Additionally, electron density difference plots show strong electron depletion in the  $\pi$ -region of the P=O double-bond (Figure 3a-d). This is probably the consequence of the interaction of the metal d-orbitals and the  $\pi$ -orbital of the P=O bond that transfers charge from the P=O double bond to the metal center, further increasing the binding of NAs to the metal center.

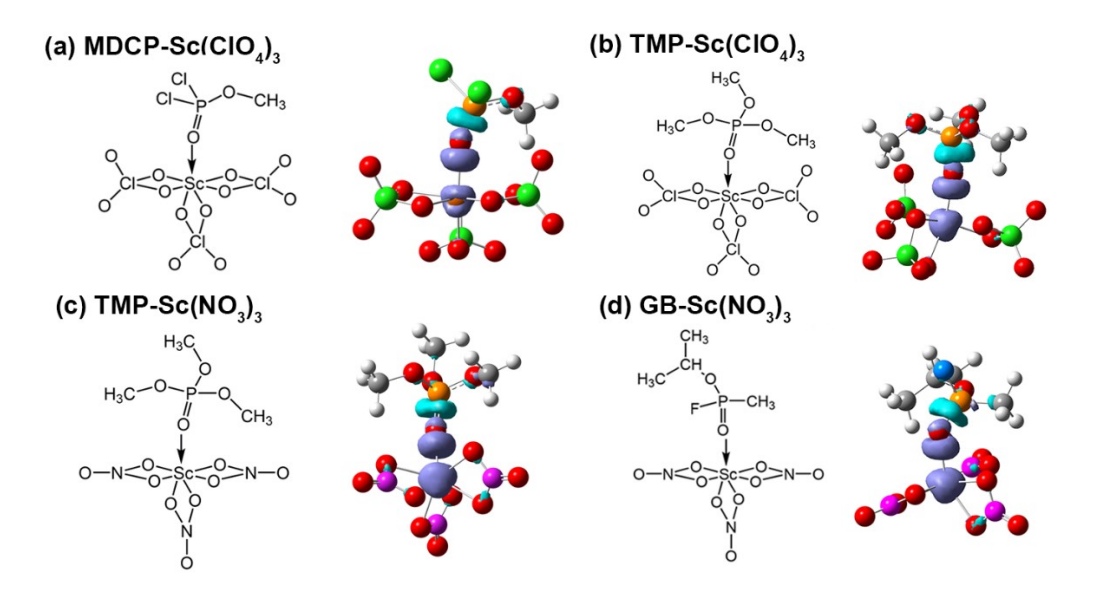


**Figure 3.** Electron-density-difference plots constructed with an isovalue of 0.005 e<sup>-</sup>/au<sup>3</sup> for (a) MDCP bound to Sc(ClO<sub>4</sub>)<sub>3</sub>, (b) TMP bound to Sc(ClO<sub>4</sub>)<sub>3</sub>, (c) TMP bound to Sc(NO<sub>3</sub>)<sub>3</sub>, and (d) GB bound to

 $Sc(NO_3)_3$ . Cyan and purple regions indicate electron-density depletion and accumulation, respectively. Atom colors: green - Cl; red - O; pink - N; dark grey - C; light silver - H; dark blue - F; dark orange - Sc; and orange - P.

3.2. Binding properties of analytes to nitrate salts and comparison of binding properties of perchlorate and nitrate salts

The  $G_{BE}$  for each analyte adsorbed to each metal-nitrate salt considered in this study is given in Figure 4. Similar to Figure 2, we order the NAs and NA simulants in Figure 4 by increasing  $\langle G_{BE}\rangle_{C, N}$  from left to right. On average over metal cations, analytes bind to nitrate salts in the following order of increasing binding strength: MDCP  $\langle DMCP \rangle \langle GA \rangle \langle GB \rangle \langle GD \rangle \langle TMP \rangle \langle DMMP \rangle \langle VX \rangle \langle DIMP$ . This is a similar order to the one mentioned in section 3.1 for perchlorate salts. Our calculated  $\langle G_{BE}\rangle_{C, N}$  values show large differences in binding strength between different NAs and NA simulants also like the case for perchlorate salts. The  $\langle G_{BE}\rangle_{C, N}$  of the weakest-binding analyte, MDCP, is 0.54 eV weaker than that of the strongest-binding analyte, DIMP (see Figure 4). Furthermore, the difference in  $G_{BE}$  among the analytes is even more significant when analyzing specific metal salts. For example, the difference in  $G_{BE}$  between the weakest and strongest binding analyte on Sc(NO<sub>3</sub>)<sub>3</sub> is 0.75 eV (see Figure 4). We also mention that Cu<sup>2+</sup> has the smallest, but still significant, difference in  $G_{BE}$  of 0.35 eV between the weakest and strongest binding analyte (see Figure 4).

The calculated values of  $\langle G_{BE} \rangle_{A, N}$  for each metal cation shown in Figure 4 reveal the following relative order of increasing binding strength:  $Cr^{3+} \langle Al^{3+} \rangle \langle Ga^{3+} \rangle \langle Cu^{2+} \rangle \langle Cd^{2+} \rangle$ 

La<sup>3+</sup> with an  $\langle G_{BE} \rangle_{A, N}$  of -1.10 eV. This difference of 0.59 eV does not vary significantly when we focus on the difference in  $G_{BE}$  between the strongest- and weakest-binding cation for a particular analyte. For example, the smallest difference in  $G_{BE}$  between the strongest- and weakest-binding cation occurs for DMCP with a difference of 0.52 eV between La<sup>3+</sup> and Cr<sup>3+</sup>. Conversely, the largest difference in  $G_{BE}$  between the strongest- and weakest-binding cations occurs for DIMP, where the  $G_{BE}$  for Sc<sup>3+</sup> is 0.73 eV stronger than that for Cu<sup>3+</sup> (see Figure 4).

	MDCP	DMCP	GA	GB	GD	TMP	DMMP	VX	DIMP	<g<sub>BE&gt;<sub>A,N</sub></g<sub>	-0.20
Cr <sup>3+</sup>	-0.20	-0.39	-0.40	-0.45	-0.43	-0.55	-0.66	-0.66	-0.83	-0.51	-0.40
Al <sup>3+</sup>	-0.20	-0.43	-0.45	-0.44	-0.44	-0.56	-0.72	-0.75	-0.75	-0.53	
Ga <sup>3+</sup>	-0.21	-0.40	-0.48	-0.46	-0.52	-0.64	-0.77	-0.73	-0.94	-0.57	-0.60
Cu <sup>2+</sup>	-0.39	-0.51	-0.57	-0.57	-0.56	-0.64	-0.75	-0.68	-0.74	-0.60	-0.80 🔵
Cd <sup>2+</sup>	-0.55	-0.72	-0.78	-0.80	-0.79	-0.84	-0.95	-0.99	-1.01	-0.83	
Fe <sup>3+</sup>	-0.57	-0.71	-0.84	-0.83	-0.88	-0.95	-1.03	-1.04	-1.23	-0.90	-1.00
Co <sup>2+</sup>	-0.60	-0.76	-0.90	-0.87	-0.90	-0.98	-1.04	-1.06	-1.03	-0.91	analytes
Zn <sup>2+</sup>	-0.65	-0.77	-0.82	-0.88	-0.92	-0.97	-1.05	-1.08	-1.09	-0.91	<del> </del>
Ni <sup>2+</sup>	-0.72	-0.86	-0.78	-0.89	-0.91	-1.02	-1.08	-1.14	-1.18	-0.95	-1.40 b
Mn <sup>2+</sup>	-0.74	-0.87	-0.94	-0.98	-1.00	-0.99	-1.19	-1.18	-1.13	-1.00	-1.60
Sc <sup>3+</sup>	-0.72	-0.87	-1.03	-1.10	-1.06	-1.02	-1.26	-1.26	-1.47	-1.09	-1.80
La <sup>3+</sup>	-0.78	-0.91	-1.03	-1.01	-0.98	-1.15	-1.30	-1.33	-1.39	-1.10	-1.00
<g<sub>BE&gt;<sub>C,N</sub></g<sub>	-0.53	-0.68	-0.75	-0.77	-0.78	-0.86	-0.98	-0.99	-1.07	-0.82	-2.00

**Figure 4.** Calculated binding free energy ( $G_{BE}$ ; in eV) for a total of nine analytes (NAs and NA simulants) on metal-nitrate salts. The color scale range is the same as in Figure 2, ranging from red (weak binding) to green (strong binding), with yellow in between. NAs and NA simulants are arranged from left to right according to increasing  $G_{BE}$  averaged over all metal cations (bottommost row,  $\langle G_{BE} \rangle_{C, N}$ ). The cations are arranged from top to bottom by increasing  $G_{BE}$  averaged over all analytes (rightmost column,  $\langle G_{BE} \rangle_{A, N}$ ).

By using the same color scale for  $G_{BE}$  in Figures 2 and 4, a direct comparison between the color grades in the two figures suggests that NAs and NA simulants bind stronger to perchlorate salts than to nitrate salts (by 0.32 eV on average). To gain more insights into the difference in binding on metal-perchlorate and -nitrate salts, we plot the  $\langle G_{BE} \rangle_{C, P}$  and  $\langle G_{BE} \rangle_{C, N}$  in Figure 5a. By ordering the analytes by increasing  $\langle |G_{BE}| \rangle_{C, P}$  or  $\langle |G_{BE}| \rangle_{C, N}$ , we find similar trends with no major

exception. We also calculate the difference between  $< G_{BE} >_{C, P}$  and  $< G_{BE} >_{C, N}$  for each analyte and find this difference to be relatively systematic, ranging from 0.27 eV to 0.37 eV.

By further analyzing the difference in binding properties of NAs and NA simulants between metal-perchlorate and metal-nitrate salts, we do not find any combination of metal cations and anions where the binding is stronger for the nitrate salt than for the respective perchlorate salt. However, we note that the differences in binding properties between metal-perchlorate and metal-nitrate salts vary largely depending on the specific choice of cation and analyte. For instance, the  $G_{BE}$  of GB for Al(ClO<sub>4</sub>)<sub>3</sub> and Al(NO<sub>3</sub>)<sub>3</sub> are -1.08 eV and -0.44 eV, respectively, a difference of 0.64 eV. Yet, the  $G_{BE}$  of GA for Cu(ClO<sub>4</sub>)<sub>3</sub> is only 0.05 eV stronger than that of Cu(NO<sub>3</sub>)<sub>3</sub>. Nevertheless, we emphasize again that this 0.05 eV difference can still be a measurable difference in carefully designed experiments. <sup>16,17,21</sup>

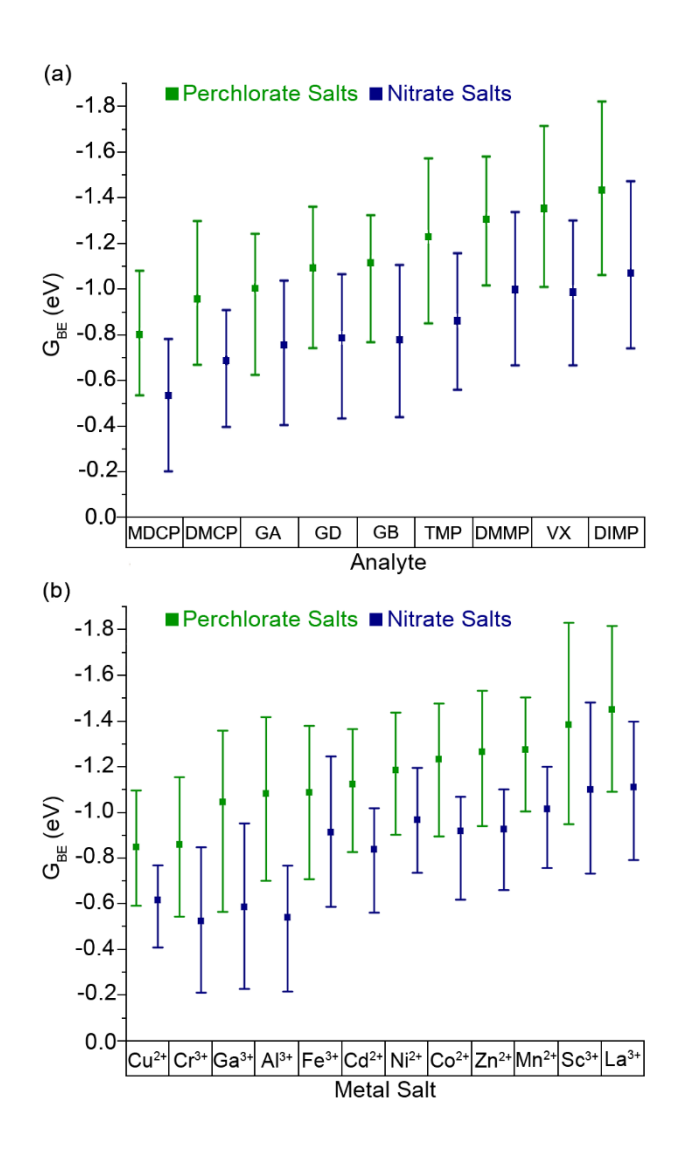


**Figure 5.** Range of calculated  $G_{BE}$  values across all (a) analytes and (b) cations for metal-perchlorate (green) and metal-nitrate (blue) salts. More negative  $G_{BE}$  corresponds to stronger binding. The ranges associated with each data point denote: (a) the numerical maximum  $G_{BE}$  for each analyte (bottom of range), the numerical minimum  $G_{BE}$  for each analyte (top of range), and the  $G_{BE}$ , or the  $G_{BE}$ , (data point in the middle of each range); (b) the numerical maximum  $G_{BE}$  for each cation (bottom of range), the numerical minimum  $G_{BE}$  for each cation (top of range), and the  $G_{BE}$ , or the  $G_{BE}$ , (data point in the middle of each range).

We also identify important trends in Figure 5b by comparing binding properties of perchlorates versus nitrates, averaged over the 9 analytes for each metal cation considered in this study:  $\langle G_{BE} \rangle_{A, P}$  and  $\langle G_{BE} \rangle_{A, N}$ . While Figure 5a emphasizes the similarities between perchlorate and nitrate salts, Figure 5b suggests considerable differences. Figure 5b is ordered by increasing  $\langle G_{BE} \rangle_{A, P}$  from

left to right and this ordering demonstrates differences between  $\langle G_{BE} \rangle_{A, N}$  and  $\langle G_{BE} \rangle_{A, P}$ . For example, the  $|\langle G_{BE} \rangle_{A, P}|$  for  $Cu^{2+}$  is the smallest for perchlorate salts, whereas the  $|\langle G_{BE} \rangle_{A, N}|$  of  $Cu^{2+}$  is larger than that for  $Cr^{3+}$ ,  $Ga^{3+}$ , and  $Al^{3+}$ . Additionally, when comparing  $Al^{3+}$  and  $Fe^{3+}$ , there is no difference between the  $\langle G_{BE} \rangle_{A, P}$ , but there is a 0.37 eV difference between the  $\langle G_{BE} \rangle_{A, N}$  on  $Al^{3+}$  and  $Fe^{3+}$ . These comparisons show that analytes can interact quite differently with metal cations in the presence of different anions due to modifications of the electronic structure of the metal cations. To visualize these differences at the electronic structure level, we present the electron-density-difference plots for TMP bound to  $Sc(ClO_4)_3$  and  $Sc(NO_3)_3$  (see Figures 3b and 3c, respectively). These plots show that electron-depletion regions (cyan) are much smaller in Figure 3c than in Figure 3b explaining why TMP binds weaker by 0.51 eV to  $Sc(NO_3)_3$  as compared to  $Sc(ClO_4)_3$ .

# 3.3. Comparison to previously published experimental results

The only available experimental work analyzing the binding properties of NAs to metal salts was published by Cadwell et al., <sup>19</sup> who used 5CB as their liquid crystal and perchlorate salts as the solid/liquid crystal interface. Figure 6 shows the comparison between our calculated displacement Gibbs Free energy (G<sub>DE</sub>) values and experimentally observed responses with a -0.35 eV threshold, using a method established in previous papers. <sup>16,21</sup> Threshold value has been introduced to account for the kinetic limitations of the displacement and compensate the simplicity of NAM that cannot otherwise be captured in these cluster models. Using this threshold, we find agreement between our calculations and experiments in 9 out of 10 cases when we use benzonitrile as a surrogate molecule for 5CB, which is similar in accuracy to our previous report comparing NAM results with experiments related to the detection of DMMP. <sup>16</sup> As previously suggested, a possible

explanation for the discrepancy between our calculations and the experiments is that modeling the open d-shell of Fe<sup>3+</sup> can be challenging.<sup>17</sup> However, another possible explanation may reflect the challenges of performing experiments with NAs. Specifically, the experiments were performed by placing drops of the NAs adjacent to the LC sensors in a closed petri dish (in a safety cabinet in a secure facility), and subsequently observing the time-dependent response of the sensors. Because the vapor pressure of VX (0.92 ppm) is lower than that of GA (49 ppm), GD (526 ppm), and GB (3816 ppm), <sup>19,53</sup> it is possible that the lower volatility of the VX led to greater variation in the concentrations of VX to which the LC sensors were exposed. In addition, there can be large variations in the air-LC partition coefficients among these analytes, which can also influence the overall kinetics of the chemoresponse significantly. These variations could lead to changes in the appropriate G<sub>DE</sub> threshold needed to predict response for different NAs, which, in turn, may explain some discrepancies between experiments and calculations.

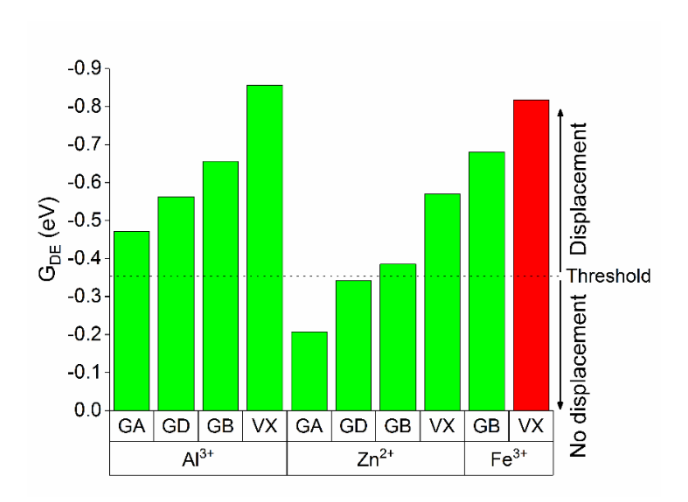


**Figure 6.** Comparison of the experimentally observed response to NAs and calculated G<sub>DE</sub> using benzonitrile as a surrogate molecule for 5CB. Displacement is predicted to occur when the G<sub>DE</sub> is -0.35 eV or more negative.<sup>19</sup> Green and red bars represent agreement and disagreement, respectively, between theoretical predictions and experimental observations in terms of displacement of LC by a given analyte (NA). Please refer to Section 3.3 for a description of how this threshold is adopted.

# 3.4. Predictions for future experiments

In section 3.3, we showed that our computational results are in good agreement with experimental observations for the detection of NAs. Furthermore, our DFT model has recently been used to guide discoveries such as that of metal-nitrate salts for the detection of DMMP,<sup>21</sup> the synthesis of mesogens that can increase chemoresponse selectivity,<sup>16</sup> and the detection of new analytes.<sup>24</sup> Therefore, our computational-chemistry calculations are capable of making important predictions that can guide future experimental efforts, the subject of this section. In the first subsection, we discuss which NA simulant is the most appropriate choice to mimic the binding strength of each NA, as a guide to safe development of NA sensors. In the second subsection, we analyze different strategies to selectively detect one particular NA from a mixture by using LC sensor arrays.<sup>54</sup>

# 3.4.1. Suitable NA simulants for specific NAs

In this study, we showed that the G<sub>BE</sub> for NAs and NA simulants can differ up to 0.88 eV for certain metal salts; thus, it is important to define basic rules for selecting appropriate NA simulants for each specific NA. Although there are numerous NA simulants, no individual one is ideal to represent all important properties of NAs such as binding to a surface, <sup>44</sup> hydrolysis, <sup>55–57</sup> air-organic partitioning, <sup>55,57</sup> vapor pressure, <sup>55,57,58</sup> and transport through metal-organic frameworks or polymer matrices. <sup>55,59</sup> Here, we suggest some simple guidelines for selecting NA simulants that best mimic a particular NA's binding properties to metal-perchlorate or metal-nitrate surfaces. However, even with these guidelines, we recommend analyzing Figure 2 and 4 in detail to find the best choice for a given metal salt, especially because 0.06 eV can lead to an order-of-magnitude difference in surface coverages. <sup>60</sup> In addition, if no suitable NA simulant exists, then we recommend using a weaker-binding simulant than the target NA, such as DMCP or MDCP, as the displacement of the

mesogen by a weaker-binding simulant would imply that displacement by all stronger-binding NAs is possible.

For each possible NA simulant-NA pair, we calculate the root-mean-square deviation (RMSD) of the G<sub>BE</sub> over all cations for metal-perchlorate and metal-nitrate salts (Figure 7). The RMSDs are used to quantify how well a NA simulant mimics the binding property of a particular NA. For the metal-perchlorate salts (Figure 7a) the best simulants for the studied NAs based on the calculated RMSD are: DMCP for GA (RMSD = 0.10 eV), DMCP or TMP for GD (RMSD = 0.16 eV for both), TMP for GB (RMSD = 0.15 eV), and DMMP for VX (RMSD = 0.09 eV). Therefore, there is a NA simulant for each NA with a RMSD less than or equal to 0.16 eV which is within DFT error (±0.2 eV).<sup>61</sup> We note that DMMP has a relatively small RMSD for VX (0.09 eV) but has a large RMSD for the other NAs ( $\geq 0.25$  eV). Thus, our calculations indicate that DMMP should be an acceptable simulant for understanding the binding properties of only VX among all NAs studied here on metal-perchlorate surfaces. We note that air-LC partition coefficients and vapor pressures of the NAs may also play an important role in deciding the most appropriate NA simulant for these LC chemoresponsive systems; these other factors are not considered in this study. Importantly, we have recently introduced simple transport models that can account for these additional factors.<sup>27,45</sup>

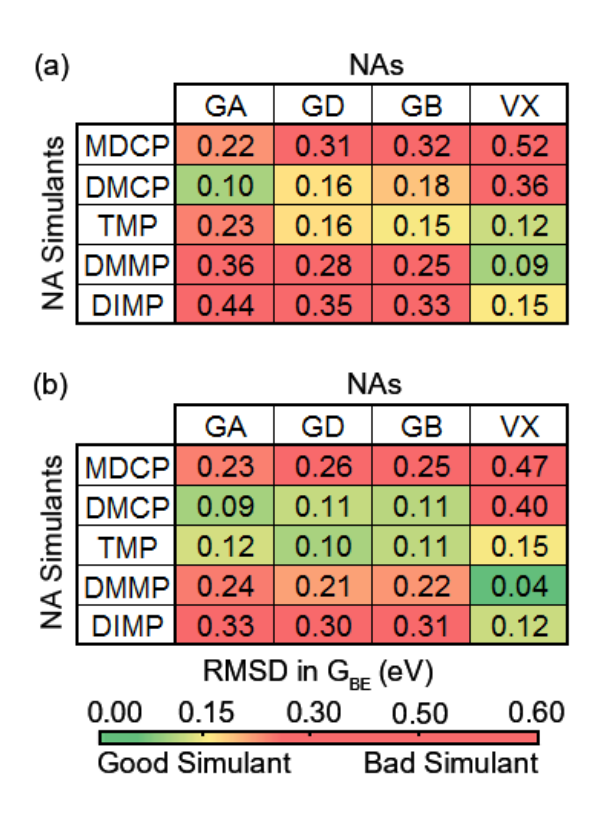


**Figure 7.** Calculated root-mean-square deviation (RMSD) in G<sub>BE</sub> for each NA-NA-simulant pairs on (a) metal-perchlorate and (b) metal-nitrate salts. Green and red shading represents a good and a bad NA simulant for a particular NA, respectively, with yellow shading for values in between.

We also calculated the RMSD in  $G_{BE}$  for each NA simulant-NA pair on metal-nitrate salts (see Figure 7b). We find that the best simulants for the studied NAs based on similar binding strength are: DMCP for GA (RMSD = 0.09 eV), TMP for GD (RMSD = 0.10 eV), DMCP or TMP for GB (RMSD = 0.11 eV for both), and DMMP for VX (RMSD = 0.04 eV). Our results show that there is a NA simulant for each NA with an RMSD of 0.11 eV or less for metal-nitrate salts. In addition, there are multiple NA simulants with RMSDs close in value to the best NA simulant-NA pair. For example, TMP is also a viable simulant for GA with an RMSD of 0.12 eV, and DMCP is also a good simulant for GD with an RMSD of 0.11 eV. We further observe that for metal-nitrate salts, DMMP is not a good NA simulant for GA, GB, or GD (RMSD > 0.20 eV), but DMMP is good

for simulating the binding of VX when metal-nitrate salts are used. In general, we find that TMP is the best overall choice if only one NA simulant is used, as it has the lowest overall error for both metal-perchlorate and metal-nitrate salts (see Figure 7).

The computational predictions of the best simulant for each NA can be rationalized by analyzing the electronegativity of NA and NA simulant functional groups as discussed earlier. For example, VX contains an ether and a sulfide group, which is similar in electronegativity to the two ether groups in DMMP, making DMMP the best simulant for VX as far as binding to salt surfaces is concerned. The best simulants for GB and GD compounds, which have one highly electronegative F ligand and one ether group, are species like TMP, which has three ether groups. TMP can compensate the highly electronegative F ligand of GB and GD with two less electronegative ether groups, making the overall binding strength comparable. Finally, GA has three electronegative functional groups: amino, cyano, and ether. The best simulant for GA is DMCP, which has three electronegative functional groups (two ether and one Cl ligands). We calculated the electron-density-difference plots for TMP (simulant for GB) and GB bound to Sc(NO<sub>3</sub>)<sub>3</sub> in Figures 3c and 3d, respectively, which shows that the electron-depletion and accumulation regions are similar in size explaining why TMP binds similarly to GB (within 0.08 eV) on Sc(NO<sub>3</sub>)<sub>3</sub>.

#### 3.4.2. Selective detection of specific NAs

In this subsection, we provide potential strategies for selectively detecting the studied NAs using an array of liquid-crystalline systems. The selective detection of NAs is important in a range of context, such as for first responders and medical personnel or to help trace the culprits of NA usage to specific organizations or countries who may have different NAs in their arsenal. We note that selectively detecting NAs from other compounds (e.g., water moisture) is also relevant; however,

this is outside of the scope of this paper. For a discussion of selective detection in the presence of water, for example, we refer the reader to two recent publications. 16,62

We analyze the displacement free energy ( $G_{DE}$ ) of NAs and NA simulants using the mesogens 5CB, PM, and PD (Scheme 1). We summarize our calculated  $G_{DE}$  results in Figure 8a-c for metal-perchlorate salts and Figure 8d-f for metal-nitrate salts. Detailed lists of results including the  $G_{BE}$  for each mesogen and the  $G_{DE}$  for each NA-simulant-mesogen pair are given in the SI (Figure S3-S9) and can serve as a database to guide future experiments. For our analysis, we employ a threshold of -0.35 eV for the  $G_{DE}$  to determine whether a displacement event will occur between the mesogen and analyte (see Section 3.3 and Figure 6). We therefore assume that displacement of the mesogen will take place by the analyte, only if the binding free energy of the analyte to the salt is stronger than that of the mesogen to the salt by at least 0.35 eV.

Using our results, we seek to highlight promising metal-salt/LC pairs for detecting different NAs, but we also encourage the reader to scrutinize Figure 8 to find other potentially viable solutions. Because detection is based on competitive binding, NAs that bind stronger than the targeted NA will always give a response if the targeted NA induces a response. Thus, selectivity in detecting particular NAs or NA simulants can be an issue. To overcome this limitation, we suggest applying sensor arrays 19,63 that include multiple independent LC systems that utilize different combinations of metal salts and/or mesogens. In principle, a sensor array can selectively detect each of the 4 NAs in this study by employing four separate LC systems. Each of the four LC systems will act independently from each other to respond to one, two, three, or all four of the studied NAs, allowing the array of LC systems to unambiguously identify a specific NA. In order to establish potential candidates for arrays of LC sensors, we first discuss the possibility of

detecting only VX, the strongest-binding NA, without detecting weaker-binding NAs. Then, we discuss the detection of two, three, and four NAs together in separate paragraphs.

The results in Figure 8 show that there are several promising LC and metal-salt combinations to selectively detect VX. For example, using Al(ClO<sub>4</sub>)<sub>3</sub>, La(ClO<sub>4</sub>)<sub>3</sub>, or Sc(ClO<sub>4</sub>)<sub>3</sub> with PD are possible systems for the selective detection of VX, as the G<sub>DE</sub> for all of the other studied NAs are above (i.e., have more positive G<sub>DE</sub>) than the required -0.35 eV threshold for displacement (Figure 8c), whereas the G<sub>DE</sub> values for VX are below (more negative G<sub>DE</sub>) this threshold. Similarly, Al(NO<sub>3</sub>)<sub>3</sub> or La(NO<sub>3</sub>)<sub>3</sub> with PM are also viable candidates with even more negative G<sub>DE</sub> values for VX (-0.57 eV and -0.65 eV, respectively) than the aforementioned metal-perchlorate salts with PD.

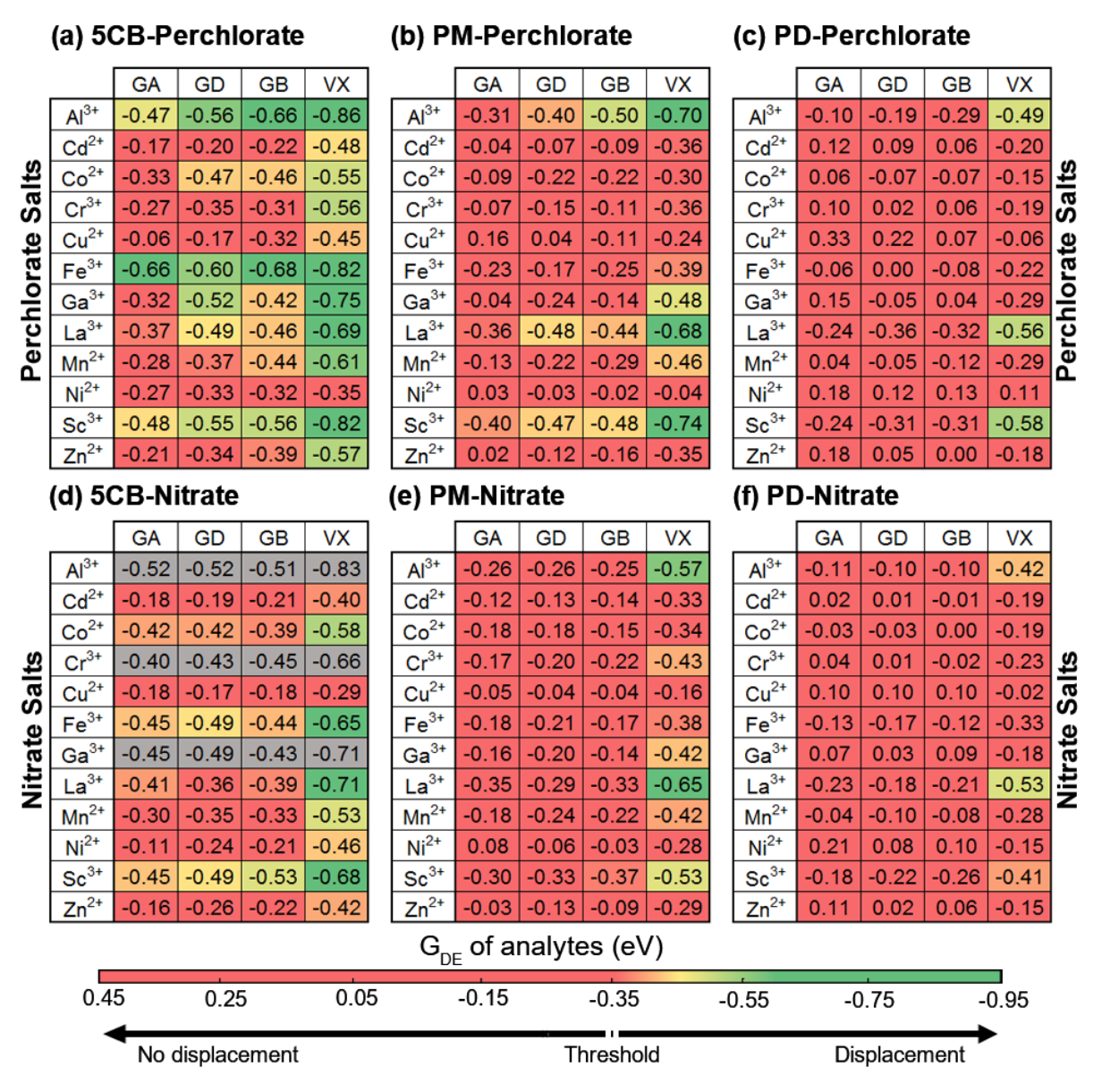


**Figure 8.** Calculated displacement Gibbs free energies ( $G_{DE}$ ; in eV) for NAs on metal-perchlorate salts with the mesogens (a) 5CB, (b) PM, and (c) PD, as well as on metal-nitrate salts with the mesogens (d) 5CB, (e) PM, and (f) PD. The color scale is the same for metal-perchlorate and metal-nitrate salts and ranges from red (no displacement predicted) to green (fast displacement predicted), while yellow and orange represent intermediate values of  $G_{DE}$  where displacement is still possible. Values shaded in gray refer to metal-salt systems where the LC is predicted to have a planar orientation and thus are not suitable for sensor applications. NAs are ordered by increasing  $<G_{BE}>_{C,Y}$  from left to right (Y = N or P), while cations are ordered alphabetically by their chemical symbols.

Finding a LC system that can respond to VX and only one other NA is difficult, because the next two weaker-binding NAs (GB and GD) have similar  $G_{BE}$  values in general (Figures 2 and 4). However, we still find a few combinations of LCs and metal-salt systems that may provide the

necessary response. Mn(ClO<sub>4</sub>)<sub>2</sub> with 5CB is a possible option, because the G<sub>DE</sub> of GB and GD differ by 0.07 eV, and the G<sub>DE</sub> of GD is close to the threshold value of -0.35 eV. Two other candidates for a LC system that responds to VX and one other NA are Ga(ClO<sub>4</sub>)<sub>3</sub> with 5CB and Al(ClO<sub>4</sub>)<sub>3</sub> with PM where the differences between the G<sub>DE</sub> of GB and GD are relatively large (0.10 eV for both) and the G<sub>DE</sub> of one NA is close to the -0.35 eV threshold. For Al(ClO<sub>4</sub>)<sub>3</sub> with PM, GD is closer to the threshold of -0.35 eV than GB; therefore, it is possible that displacement occurs only for GB and VX and not for GD. In the case of Ga(ClO<sub>4</sub>)<sub>3</sub> with 5CB, GB is closer to the threshold of -0.35 eV than GD (the G<sub>DE</sub> of GD and GB is -0.52 and -0.42 eV, respectively); as such, the displacement may occur only for GD and VX and not for GB. Thus, it might be possible to find a LC system that can detect either VX and GD or VX and GB. We note that these candidates are not perfect and that it is possible that all of the described systems will respond to GB, GD, and VX because the G<sub>DE</sub> of these systems are all at least slightly below (i.e., more negative) the -0.35 eV threshold. To create LC systems that distinguish between GB and GD, one may have to find another stronger-binding mesogen that can shift the G<sub>DE</sub> of the NAs for Mn(ClO<sub>4</sub>), Ga(ClO<sub>4</sub>), Al(ClO<sub>4</sub>), or other metal salts into the range where a positive response to all three NAs is circumvented by pushing the G<sub>DE</sub> of either GB or GD above the G<sub>DE</sub> threshold. Finding such a mesogen is outside the scope of this work, but we have shown successful examples previously by designing PM and PD mesogens using computational chemistry predictions to increase the humidity tolerance of chemoresponsive LC systems.<sup>16</sup>

A LC sensor design based on  $Co(ClO_4)_2$  and 5CB appears promising for simultaneous detection of VX, GB, and GD. The  $G_{DE}$  of VX, GB, and GD are -0.55, -0.46, -0.47 eV, respectively, which are all reasonably below the threshold of -0.35 eV, whereas the  $G_{DE}$  of GA is only -0.33 eV. Other potentially viable candidates are  $La(ClO_4)_3$  with 5CB or  $Sc(ClO_4)_3$  with PM. In these cases,

however, the G<sub>DE</sub> of GA are somewhat below the threshold (-0.37 eV and -0.40 eV, respectively), which can cause detection problems by providing false-positive results.

Finally, we mention that Al(ClO<sub>4</sub>)<sub>3</sub> with 5CB, Fe(ClO<sub>4</sub>)<sub>3</sub> with 5CB, and Sc(ClO<sub>4</sub>)<sub>3</sub> with 5CB are the best candidates to detect all four NAs without any selectivity among them. In these three systems, the weakest-binding NA has a G<sub>DE</sub> value of -0.47, -0.60, and -0.48 eV, respectively, suggesting an easy displacement of the mesogen by all NAs. Good candidates for the detection of all four NAs with metal-nitrate salts include Fe(NO<sub>3</sub>)<sub>3</sub> with 5CB and Sc(NO<sub>3</sub>)<sub>3</sub> with 5CB, where the weakest-binding NAs have G<sub>DE</sub> values of -0.45 eV in both systems. However, metal-perchlorate salts may be preferred over metal-nitrate salts based on previous studies which show that humidity can influence the observed response times for certain metal-nitrate salts.<sup>21</sup>

#### 4. CONCLUSIONS

In this study, motivated by the utility of metal salts as binding sites for design of materials for NA capture, destruction, and sensing, we employed DFT calculations to analyze the binding properties of four NAs and five NA simulants on twelve metal-perchlorate and twelve metal-nitrates salt surfaces. The key result reported in this paper is that there are large differences in the binding strength of the studied NAs and NA simulants across different metal salts. Thus, our study highlights the importance of computational high throughput screening to design the next generation materials for NA capture, destruction, and sensing particularly because the toxicity and limited availability of NAs makes experimental efforts challenging.

The observed large differences in the binding strength also indicate that there is no individual NA simulant that correctly describes the adsorption behavior of all NAs on metal salts. Importantly, the comparison of NAs with NA simulants has to be treated carefully, as certain

physico-chemical similarities do not necessarily guarantee that NA simulants behave similarly to

NAs when binding to metal salts. To guide future experimental efforts, we established a general

trend in the binding strength of NAs and their simulants independent from the metal salt in the

following increasing order: MDCP < DMCP < GA < GD ~ GB < TMP < VX ~ DMMP < DIMP.

Building on this trend, we show that the best NA/NA simulant pairs based on similar G<sub>BE</sub> to both

metal-nitrate and -perchlorate salts are: GA/DMCP, GD/TMP, GB/TMP, and VX/DMMP.

We also move one step further to show how computational high throughput screening can be

used for NA sensor design building on the example of liquid crystals-based chemoresponsive

systems. Our high throughput results serve as a guide for future experiments and provide a rich

database including promising combinations of liquid-crystal and metal-salt systems to selectively

detect NAs using, e.g., sensor arrays. In addition, we demonstrated that our computational

chemistry predictions show good agreement with available experimental data, suggesting that

electronic structure methods can be of great value in designing selective sensors for NAs detection.

ASSOCIATED CONTENT

**Supporting Information** 

Gibbs free binding energies for NAs, NA simulants, and mesogens on metal-perchlorate and metal-

nitrate salts, displacement Gibbs free energies for all NAs and NA simulants with respect to 5CB,

PM, and PD.

AUTHOR INFORMATION

Corresponding Author: Manos Mavrikakis (emavrikakis@wisc.edu)

34

# Acknowledgement

J.I.G., T.S., N.L.A., and M.M.'s work was supported by the National Science Foundation (DMR-1921722) and the Army Research Office (W911NF-14-1-0140). J.I.G., T.S., and M.M.'s computational work was carried at various computing centers through the DoD High Performance Computing Modernization Program (US Air Force Research Laboratory DoD Supercomputing Resource Center (AFRL DSRC), the US Army Engineer Research and Development Center (ERDC), and the Navy DoD Supercomputing Resource Center (Navy DSRC), ARONC43623362), all supported by the US Department of Defense. We thank Benjamin W. J. Chen, Ahmed O. Elnabawy, Ellen A. Murray, and Sean A. Tacey for helpful comments and discussion.

#### References

- (1) Kimball, D. G. The Chemical Wapons Convention (CWC) at a Glance https://www.armscontrol.org/factsheets/cwcglance.
- (2) Durisic, M. P.; Tafa, Z.; Dimic, G.; Milutinovic, V. A Survey of Military Applications of Wireless Sensor Networks. *Mediterr. Conf. Embed. Comput.* **2012**, 196–199.
- (3) Hu, X.-X. X.; Su, Y.-T. T.; Ma, Y.-W. W.; Zhan, X.-Q. Q.; Zheng, H.; Jiang, Y.-B. B. A near Infrared Colorimetric and Fluorometric Probe for Organophosphorus Nerve Agent Mimics by Intramolecular Amidation. *Chem. Commun.* 2015, 51 (82), 15118–15121. https://doi.org/10.1039/c5cc04630k.

- (4) National Research Council. *Monitoring at Chemical Agent Disposal Facilities*; The National Academies Press: Washington, DC, 2005.
- (5) Black, R. M.; Clarke, R. J.; Read, R. W.; Reid, M. T. J. Application of Gas Chromatography-Mass Spectrometry and Gas Chromatography-Tandem Mass Spectrometry to the Analysis of Chemical Warfare Samples, Found to Contain Residues of the Nerve Agent Sarin, Sulphur Mustard and Their Degradation Products. *J. Chromatogr. A* **1994**, *662* (2), 301–321. https://doi.org/10.1016/0021-9673(94)80518-0.
- (6) Severin, E. J.; Doleman, B. J.; Lewis, N. S. An Investigation of the Concentration Dependence and Response to Analyte Mixtures of Carbon Black/Insulating Organic Polymer Composite Vapor Detectors. *Anal. Chem.* 2000, 72 (4), 658–668. https://doi.org/10.1021/ac9910278.
- (7) Hopkins, A. R.; Lewis, N. S. Detection and Classification Characteristics of Arrays of Carbon Black/Organic Polymer Composite Chemiresistive Vapor Detectors for the Nerve Agent Simulants Dimethylmethylphosphonate and Diisopropylmethylphosponate. *Anal. Chem.* **2001**, *73* (5), 884–892. https://doi.org/10.1021/ac0008439.
- (8) Bencic-Nagale, S.; Sternfeld, T.; Walt, D. R. Microbead Chemical Switches: An Approach to Detection of Reactive Organophosphate Chemical Warfare Agent Vapors. *J. Am. Chem. Soc.* **2006**, *128* (15), 5041–5048. https://doi.org/10.1021/ja057057b.
- (9) Walker, J. P.; Asher, S. A. Acetylcholinesterase-Based Organophosphate Nerve Agent Sensing Photonic Crystal. *Anal. Chem.* **2005**, 77 (6), 1596–1600. https://doi.org/10.1021/ac048562e.

- (10) Zhang, S. W.; Swager, T. M. Fluorescent Detection of Chemical Warfare Agents: Functional Group Specific Ratiometric Chemosensors. *J. Am. Chem. Soc.* **2003**, *125* (12), 3420–3421. https://doi.org/10.1021/ja029265z.
- (11) Kim, K.; Tsay, O. G.; Atwood, D. A.; Churchill, D. G. Destruction and Detection of Chemical Warfare Agents. *Chem. Rev.* **2011**, *111* (9), 5345–5403. https://doi.org/10.1021/cr100193y.
- (12) Katz, M. J.; Mondloch, J. E.; Totten, R. K.; Park, J. K.; Nguyen, S. T.; Farha, O. K.; Hupp, J. T. Simple and Compelling Biomimetic Metal-Organic Framework Catalyst for the Degradation of Nerve Agent Simulants. *Angew. Chemie Int. Ed.* 2014, 53 (2), 497–501. https://doi.org/10.1002/anie.201307520.
- (13) Moon, S. Y.; Liu, Y.; Hupp, J. T.; Farha, O. K. Instantaneous Hydrolysis of Nerve-Agent Simulants with a Six-Connected Zirconium-Based Metal-Organic Framework. *Angew. Chemie Int. Ed.* **2015**, *54* (23), 6795–6799. https://doi.org/10.1002/anie.201502155.
- (14) Mahato, T. H.; Prasad, G. K.; Singh, B.; Acharya, J.; Srivastava, A. R.; Vijayaraghavan, R. Nanocrystalline Zinc Oxide for the Decontamination of Sarin. *J. Hazard. Mater.* **2009**, *165* (1–3), 928–932. https://doi.org/10.1016/j.jhazmat.2008.10.126.
- (15) O'Shea, K. E.; Beightol, S.; Garcia, I.; Aguilar, M.; Kalen, D. V.; Cooper, W. J. Photocatalytic Decomposition of Organophosphonates in Irradiated TiO<sub>2</sub> Suspensions. *J. Photochem. Photobiol. A Chem.* 1997, 107 (1–3), 221–226. https://doi.org/10.1016/S1010-6030(96)04420-6.
- (16) Yu, H.; Szilvási, T.; Rai, P.; Twieg, R. J.; Mavrikakis, M.; Abbott, N. L. Computational

- Chemistry-Guided Design of Selective Chemoresponsive Liquid Crystals Using Pyridine and Pyrimidine Functional Groups. *Adv. Funct. Mater.* **2018**, *28* (13), 1703581. https://doi.org/10.1002/adfm.201703581.
- (17) Szilvási, T.; Roling, L. T.; Yu, H.; Rai, P.; Choi, S.; Twieg, R. J.; Mavrikakis, M.; Abbott, N. L. Design of Chemoresponsive Liquid Crystals through Integration of Computational Chemistry and Experimental Studies. *Chem. Mater.* 2017, 29 (8), 3563–3571. https://doi.org/10.1021/acs.chemmater.6b05430.
- (18) Nayani, K.; Rai, P.; Bao, N.; Yu, H.; Mavrikakis, M.; Twieg, R. J.; Abbott, N. L. Liquid Crystals with Interfacial Ordering That Enhances Responsiveness to Chemical Targets. *Adv. Mater.* **2018**, *30* (27), 1–7. https://doi.org/10.1002/adma.201706707.
- (19) Cadwell, K. D.; Lockwood, N. A.; Nellis, B. A.; Alf, M. E.; Willis, C. R.; Abbott, N. L. Detection of Organophosphorous Nerve Agents Using Liquid Crystals Supported on Chemically Functionalized Surfaces. *Sensors Actuators B Chem.* 2007, 128 (1), 91–98. https://doi.org/10.1016/j.snb.2007.05.044.
- (20) Pearson, R. G. Hard and Soft Acids and Bases, Part 1: Fundamental Principles. *J. Chem. Educ.* **1968**, *45* (9), 581–587. https://doi.org/https://doi.org/10.1021/ed045p581.
- (21) Szilvási, T.; Bao, N.; Yu, H.; Twieg, R. J.; Mavrikakis, M.; Abbott, N. L. The Role of Anions in Adsorbate-Induced Anchoring Transitions of Liquid Crystals on Surfaces with Discrete Cation Binding Sites. *Soft Matter* 2018, 14 (5), 797–805. https://doi.org/10.1039/C7SM01981E.
- (22) Cadwell, K. D.; Alf, M. E.; Abbott, N. L. Infrared Spectroscopy of Competitive Interactions

- between Liquid Crystals, Metal Salts, and Dimethyl Methylphosphonate at Surfaces. *J. Phys. Chem. B* **2006**, *110* (51), 26081–26088. https://doi.org/10.1021/jp063211k.
- (23) Shah, R. R.; Abbott, N. L. Principles for Measurement of Chemical Exposure Based on Recognition-Driven Anchoring Transitions in Liquid Crystals. *Science* **2001**, *293* (5533), 1296–1299. https://doi.org/10.1126/science.1062293.
- (24) Szilvási, T.; Bao, N.; Nayani, K.; Yu, H.; Rai, P.; Twieg, R. J.; Mavrikakis, M.; Abbott, N. L. Redox-Triggered Orientational Responses of Liquid Crystals to Chlorine Gas. *Angew. Chemie Int. Ed.* 2018, 57 (31), 9665–9669. https://doi.org/10.1002/anie.201803194.
- (25) Roling, L. T.; Scaranto, J.; Herron, J. A.; Yu, H.; Choi, S.; Abbott, N. L.; Mavrikakis, M. Towards First-Principles Molecular Design of Liquid Crystal-Based Chemoresponsive Systems. *Nat. Commun.* **2016**, *7*, 13338. https://doi.org/10.1038/ncomms13338.
- (26) Hunter, J. T.; Abbott, N. L. Adsorbate-Induced Anchoring Transitions of Liquid Crystals on Surfaces Presenting Metal Salts with Mixed Anions. ACS Appl. Mater. Interfaces 2014, 6 (4), 2362–2369. https://doi.org/10.1021/am404632r.
- (27) Hunter, J. T.; Abbott, N. L. Dynamics of the Chemo-Optical Response of Supported Films of Nematic Liquid Crystals. *Sensors Actuators B Chem.* **2013**, *183*, 71–80. https://doi.org/10.1016/j.snb.2013.03.094.
- (28) Wang, P.-H.; Yu, J.-H.; Zhao, Y.-B.; Li, Z.-J.; Li, G.-Q. A Novel Liquid Crystal-Based Sensor for the Real-Time Identification of Organophosphonate Vapors. *Sensors Actuators B Chem.* **2011**, *160* (1), 929–935. https://doi.org/10.1016/j.snb.2011.09.005.
- (29) Bungabong, M. L.; Ong, P. Bin; Yang, K. L. Using Copper Perchlorate Doped Liquid

- Crystals for the Detection of Organophosphonate Vapor. *Sensors Actuators, B Chem.* **2010**, 148 (2), 420–426. https://doi.org/10.1016/j.snb.2010.05.063.
- Yang, K.-L.; Cadwell, K.; Abbott, N. L. Use of Self-Assembled Monolayers, Metal Ions and Smectic Liquid Crystals to Detect Organophosphonates. *Sensors Actuators B Chem.* 2005, 104 (1), 50–56. https://doi.org/10.1016/j.snb.2004.04.098.
- (31) Yang, K.; Cadwell, K.; Abbott, N. L. Mechanistic Study of the Anchoring Behavior of Liquid Crystals Supported on Metal Salts and Their Orientational Responses to Dimethyl Methylphosphonate. J. Phys. Chem. B 2004, 108 (52), 20180–20186. https://doi.org/10.1021/jp0470391.
- (32) Loudet, J. C.; Poulin, P. Application of an Electric Field to Colloidal Particles Suspended in a Liquid-Crystal Solvent. *Phys. Rev. Lett.* **2001**, 87 (16), 165503. https://doi.org/10.1103/PhysRevLett.87.165503.
- (33) Yokoyama, H.; van Sprang, H. A. A Novel Method for Determining the Anchoring Energy Function at a Nematic Liquid Crystal-wall Interface from Director Distortions at High Fields. *J. Appl. Phys.* **1985**, *57* (10), 4520–4526. https://doi.org/10.1063/1.335352.
- (34) Schadt, M.; Helfrich, W. Voltage-Dependent Optical Activity of a Twisted Nematic Liquid Crystal. *Appl. Phys. Lett.* **1971**, *18* (4), 127–128. https://doi.org/10.1063/1.1653593.
- Robinson, S. E.; Grinwald, B. A.; Bremer, L. L.; Kupcho, K. A.; Acharya, B. R.; Owens, P. D. A Liquid Crystal-Based Passive Badge for Personal Monitoring of Exposure to Hydrogen Sulfide. *J. Occup. Environ. Hyg.* 2014, 11 (11), 741–750. https://doi.org/10.1080/15459624.2014.916808.

- (36) Sen, A.; Kupcho, K. A.; Grinwald, B. A.; VanTreeck, H. J.; Acharya, B. R. Liquid Crystal-Based Sensors for Selective and Quantitative Detection of Nitrogen Dioxide. *Sensors Actuators B Chem.* **2013**, *178*, 222–227. https://doi.org/10.1016/j.snb.2012.12.036.
- (37) Stumpel, J. E.; Wouters, C.; Herzer, N.; Ziegler, J.; Broer, D. J.; Bastiaansen, C. W. M.; Schenning, A. P. H. J. An Optical Sensor for Volatile Amines Based on an Inkjet-Printed, Hydrogen-Bonded, Cholesteric Liquid Crystalline Film. *Adv. Opt. Mater.* **2014**, *2* (5), 459–464. https://doi.org/10.1002/adom.201300516.
- (38) Han, Y.; Pacheco, K.; Bastiaansen, C. W. M.; Broer, D. J.; Sijbesma, R. P. Optical Monitoring of Gases with Cholesteric Liquid Crystals. *J. Am. Chem. Soc.* **2010**, *132* (9), 2961–2967. https://doi.org/10.1021/ja907826z.
- (39) Yu, H.; Szilvási, T.; Wang, K.; Gold, J. I.; Bao, N.; Twieg, R. J.; Mavrikakis, M.; Abbott, N. L. Amplification of Elementary Surface Reaction Steps on Transition Metal Surfaces Using Liquid Crystals: Dissociative Adsorption and Dehydrogenation. *J. Am. Chem. Soc.* 2019, 141 (40), 16003–16013. https://doi.org/10.1021/jacs.9b08057.
- (40) Yang, K.-L.; Cadwell, K.; Abbott, N. L. Contact Printing of Metal Ions onto Carboxylate-Terminated Self-Assembled Monolayers. *Adv. Mater.* **2003**, *15* (21), 1819–1823. https://doi.org/10.1002/adma.200305478.
- (41) Pal, S. K.; Acevedo-Vélez, C.; Hunter, J. T.; Abbott, N. L. Effects of Divalent Ligand Interactions on Surface-Induced Ordering of Liquid Crystals. *Chem. Mater.* 2010, 22 (19), 5474–5482. https://doi.org/10.1021/cm1011058.
- (42) Panayotov, D. A.; Morris, J. R. Uptake of a Chemical Warfare Agent Simulant (DMMP)

- on TiO<sub>2</sub>: Reactive Adsorption and Active Site Poisoning. *Langmuir* **2009**, *25* (6), 3652–3658. https://doi.org/10.1021/la804018b.
- (43) Bermudez, V. M. Computational Study of the Adsorption of Trichlorophosphate, Dimethyl Methylphosphonate, and Sarin on Amorphous SiO<sub>2</sub>. *J. Phys. Chem. C* **2007**, *111* (26), 9314–9323. https://doi.org/10.1021/jp071529m.
- (44) Davis, E. D.; Gordon, W. O.; Wilmsmeyer, A. R.; Troya, D.; Morris, J. R. Chemical Warfare Agent Surface Adsorption: Hydrogen Bonding of Sarin and Soman to Amorphous Silica. *J. Phys. Chem. Lett.* **2014**, *5* (8), 1393–1399. https://doi.org/10.1021/jz500375h.
- (45) Sheavly, J. K.; Gold, J. I.; Mavrikakis, M.; Van Lehn, R. C. Molecular Simulations of Analyte Partitioning and Diffusion in Liquid Crystal Sensors. *Mol. Syst. Des. Eng.* 2020, 5 (1), 304–316. https://doi.org/10.1039/c9me00126c.
- Gaussian 09, Revision D.01, M. J. Frisch, G. W. Trucks, H. B. Schlegel, G. E. Scuseria, M. A. Robb, J. R. Cheeseman, G. Scalmani, V. Barone, B. Mennucci, G. A. Petersson, H. Nakatsuji, M. Caricato, X. Li, H. P. Hratchian, A. F. Izmaylov, J. Bloino, G. Zheng, J. L. Sonnenberg, M. Hada, M. Ehara, K. Toyota, R. Fukuda, J. Hasegawa, M. Ishida, T. Nakajima, Y. Honda, O. Kitao, H. Nakai, T. Vreven, J. A. Montgomery, Jr., J. E. Peralta, F. Ogliaro, M. Bearpark, J. J. Heyd, E. Brothers, K. N. Kudin, V. N. Staroverov, R. Kobayashi, J. Normand, K. Raghavachari, A. Rendell, J. C. Burant, S. S. Iyengar, J. Tomasi, M. Cossi, N. Rega, J. M. Millam, M. Klene, J. E. Knox, J. B. Cross, V. Bakken, C. Adamo, J. Jaramillo, R. Gomperts, R. E. Stratmann, O. Yazyev, A. J. Austin, R. Cammi, C. Pomelli, J. W. Ochterski, R. L. Martin, K. Morokuma, V. G. Zakrzewski, G. A. Voth, P. Salvador, J. J. Dannenberg, S. Dapprich, A. D. Daniels, Ö. Farkas, J. B. Foresman, J. V. Ortiz, J.

# Cioslowski, and D. J. Fox, Gaussian, Inc., Wallingford CT, 2009.

- Revision, D.; Frisch, M. J.; Trucks, G. W.; Schlegel, H. B.; Scuseria, G. E.; Robb, A.; Cheeseman, J. R.; Scalmani, G.; Barone, V.; Mennucci, B.; et al. Gaussian 09, Revision. *Gaussian 09, Revis. D.01; Gaussian, Inc. Wallingford, CT*, **2015**, 1–20.
- (47) Perdew, J. P.; Burke, K.; Ernzerhof, M. Generalized Gradient Approximation Made Simple.

  Phys. Rev. Lett. 1996, 77 (18), 3865–3868. https://doi.org/10.1103/PhysRevLett.77.3865.
- (48) Grimme, S.; Antony, J.; Ehrlich, S.; Krieg, H. A Consistent and Accurate Ab Initio Parametrization of Density Functional Dispersion Correction (DFT-D) for the 94 Elements H-Pu. *J. Chem. Phys.* **2010**, *132* (15), 154104. https://doi.org/10.1063/1.3382344.
- (49) Weigend, F.; Ahlrichs, R. Balanced Basis Sets of Split Valence, Triple Zeta Valence and Quadruple Zeta Valence Quality for H to Rn: Design and Assessment of Accuracy. *Phys. Chem. Chem. Phys.* **2005**, *7* (18), 3297. https://doi.org/10.1039/b508541a.
- (50) Zhao, Y.; Truhlar, D. G. The M06 Suite of Density Functionals for Main Group Thermochemistry, Thermochemical Kinetics, Noncovalent Interactions, Excited States, and Transition Elements: Two New Functionals and Systematic Testing of Four M06-Class Functionals and 12 Other Function. *Theor. Chem. Acc.* 2008, 120 (1–3), 215–241. https://doi.org/10.1007/s00214-007-0310-x.
- (51) Wilmsmeyer, A. R.; Gordon, W. O.; Davis, E. D.; Troya, D.; Mantooth, B. A.; Lalain, T. A.; Morris, J. R. Infrared Spectra and Binding Energies of Chemical Warfare Nerve Agent Simulants on the Surface of Amorphous Silica. *J. Phys. Chem. C* 2013, *117* (30), 15685–15697. https://doi.org/10.1021/jp404265s.

- (52) Yang, K. L.; Cadwell, K.; Abbott, N. L. Mechanistic Study of the Anchoring Behavior of Liquid Crystals Supported on Metal Salts and Their Orientational Responses to Dimethyl Methylphosphonate. J. Phys. Chem. B 2004, 108 (52), 20180–20186. https://doi.org/10.1021/jp0470391.
- (53) Hoenig, S. L. Compendium of Chemical Warfare Agents; Springer: New York, 2006. https://doi.org/10.1007/978-0-387-69260-9.
- (54) Srivastava, A. K. Detection of Volatile Organic Compounds (VOCs) Using SnO<sub>2</sub> Gas-Sensor Array and Artifical Neural Network. *Sensors Actuators B Chem.* **2003**, *96* (1–2), 24–37. https://doi.org/10.1016/S0925-4005(03)00477-5.
- (55) Bartelt-Hunt, S. L.; Knappe, D. R. U.; Barlaz, M. A. A Review of Chemical Warfare Agent Simulants for the Study of Environmental Behavior. *Crit. Rev. Environ. Sci. Technol.* **2008**, 38 (2), 112–136. https://doi.org/10.1080/10643380701643650.
- (56) Yang, Y. C. Chemical Detoxification of Nerve Agent VX. Acc. Chem. Res. 1999, 32 (2), 109–115. https://doi.org/10.1021/ar970154s.
- (57) Munro, N. B.; Ambrose, K. R.; Watson, A. P. Toxicity of the Organophosphate Chemical Warfare Agents GA, GB, and VX: Implications for Public Protection. *Environ. Health Perspect.* **1994**, *102* (1), 18–38. https://doi.org/10.1289/ehp.9410218.
- (58) Fatah, A. A.; Arcilesi, R.; Judd, A.; O'Connor, L.; Lattin, C. H.; Wells, C. Y. Guide for the Selection of Chemical and Biological Decontamination Equipment for Emergency First Responders; 2007.
- (59) Agrawal, M.; Boulfelfel, S. E.; Sava Gallis, D. F.; Greathouse, J. A.; Sholl, D. S.

- Determining Diffusion Coefficients of Chemical Warfare Agents in Metal-Organic Frameworks. *J. Phys. Chem. Lett.* **2019**, *10* (24), 7823–7830. https://doi.org/10.1021/acs.jpclett.9b03119.
- (60) Tacey, S. A.; Xu, L.; Szilvási, T.; Schauer, J. J.; Mavrikakis, M. Quantum Chemical Calculations to Determine Partitioning Coefficients for HgCl<sub>2</sub> on Iron-Oxide Aerosols. *Sci. Total Environ.* **2018**, *636*, 580–587. https://doi.org/10.1016/j.scitotenv.2018.04.289.
- (61) Norskov, J. K.; Abild-Pedersen, F.; Studt, F.; Bligaard, T. Density Functional Theory in Surface Chemistry and Catalysis. *Proc. Natl. Acad. Sci.* **2011**, *108* (3), 937–943. https://doi.org/10.1073/pnas.1006652108.
- (62) Cao, Y.; Yu, H.; Abbott, N. L.; Zavala, V. M. Machine Learning Algorithms for Liquid Crystal-Based Sensors. *ACS Sensors* **2018**, *3*, 2237–2245. https://doi.org/10.1021/acssensors.8b00100.
- (63) Acharya, B.; Sen, A.; Abbott, N.; Kupcho, K. Detection of Vapor Phase Compounds by Changes in Physical Properties of a Liquid Crystal. 8178355, 2012.

# **GRAPHICAL ABSTRACT:**

